



# Interface Embrittlement Between 63Sn-37Pb Solder and Au Layer—Part 1: Physical Metallurgy of Liquid-State and Solid-State Reactions

P. T. Vianco<sup>1</sup> · A. C. Kilgo<sup>1</sup> · B. M. McKenzie<sup>1</sup> · R. L. Grant<sup>1</sup> · S. Williams<sup>1</sup>

Received: 5 March 2022 / Accepted: 10 August 2022 / Published online: 30 August 2022

This is a U.S. Government work and not under copyright protection in the US; foreign copyright protection may apply 2022

## Abstract

This study examined the interface microstructure that developed between 63Sn-37Pb (Sn-Pb) solder and the Au protective layer that was not fully consumed during the soldering process. This scenario leads to a Au interface embrittlement failure mode that places at risk high-reliability electronics using the eutectic Sn-Pb solder and Au protective finishes. The sessile drop test sample assessed the roles of solder thickness and solid-state aging (55–100°C; 5–40 days). The interface microstructure began with a contiguous, secondary Au-Sn intermetallic compound (IMC) layer adjacent to the Au layer and an accumulation of particles that would coarsen into the primary Au-Sn IMC layer next to the solder. The baseline condition, which was established by aging for 28 days at 25°C, caused a noticeable increase of Kirkendall voids along the Au/secondary Au-Sn IMC interface. The following trend was observed: Kirkendall voids increased with decreasing solder thickness. The risk of catastrophic failure was high when the solder thickness was < 50 µm; the risk was low when the solder thickness was > 100 µm. The thick solder layer also caused Kirkendall voids to develop within the secondary Au-Sn IMC grain structure and extended into the primary Au-Sn IMC layer. However, these voids posed a low risk to solder joint integrity. The Au interface embrittlement mechanism, which results from the incomplete removal of a Au protective finish, can lead to infant mortality failures prior to, or latent failures after, the solder joint has entered service.

**Keywords** Gold · interface embrittlement · Kirkendall voids · solid-state aging

## Introduction

### Au Embrittlement Mechanisms

Gold (Au) promotes the wetting and spreading of tin (Sn)-based solders.<sup>1–3</sup> Functionally, the Au coating serves as the protective layer when deposited over a nickel (Ni) solderable layer. Figure 1 illustrates the following soldering process steps. Molten solder initially wets and spreads over the Au surface. The Au layer is dissolved into the molten solder (dotted arrows). Then, the solder wets the pristine Ni surface. A small quantity of Ni is dissolved into the solder (white arrows). The Sn component of the solder creates a metallurgical bond with the Ni layer by the formation of a Ni-Sn intermetallic compound (IMC) layer. The typical

thicknesses of the Au and Ni layers are 1.3–2.5 µm and 1.3–3.8 µm, respectively, when typically deposited by electroplating practices.<sup>4</sup>

The use of a Au protective layer heightens the risk of solder joint embrittlement. Gold and Sn combine in the solder to form one or more Au<sub>x</sub>Sn<sub>y</sub> IMCs, which when present in a sufficient quantity, reduce the ductility of the solder [2]. This bulk embrittlement phenomenon was recognized more than 50 years ago. Bester et al. found that Au concentrations in excess of 4 wt.% caused a significant reduction in ductility of eutectic tin-Pb (Sn-Pb) solder.<sup>5</sup> The so-called four-percent rule was established as the maximum Au concentration allowable in Sn-Pb solder joints to avoid the bulk embrittlement failure mode.

The immersion (conversion) Au layer was introduced into printed circuit board applications. The immersion Au protective layer first appeared in combination with an electroless Ni(P) protective layer (3–6 µm thick) to create the electroless Ni/immersion Au or “ENIG” surface finish.<sup>6</sup> Solderability protection was provided by the very dense microstructure of

✉ P. T. Vianco  
ptvianco@gmail.com

<sup>1</sup> Sandia National Laboratories, Albuquerque, NM, USA

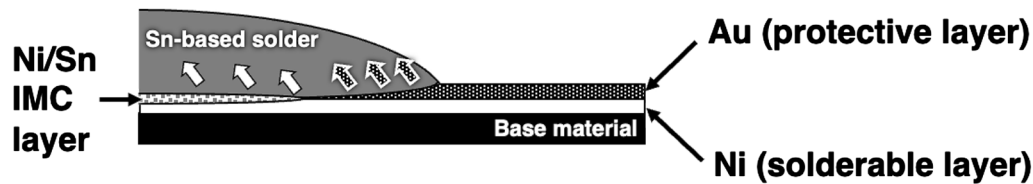


**Fig. 1** Schematic diagram illustrates the wetting and spreading of molten solder over a surface finish comprising a Ni solderable layer and Au protective layer.

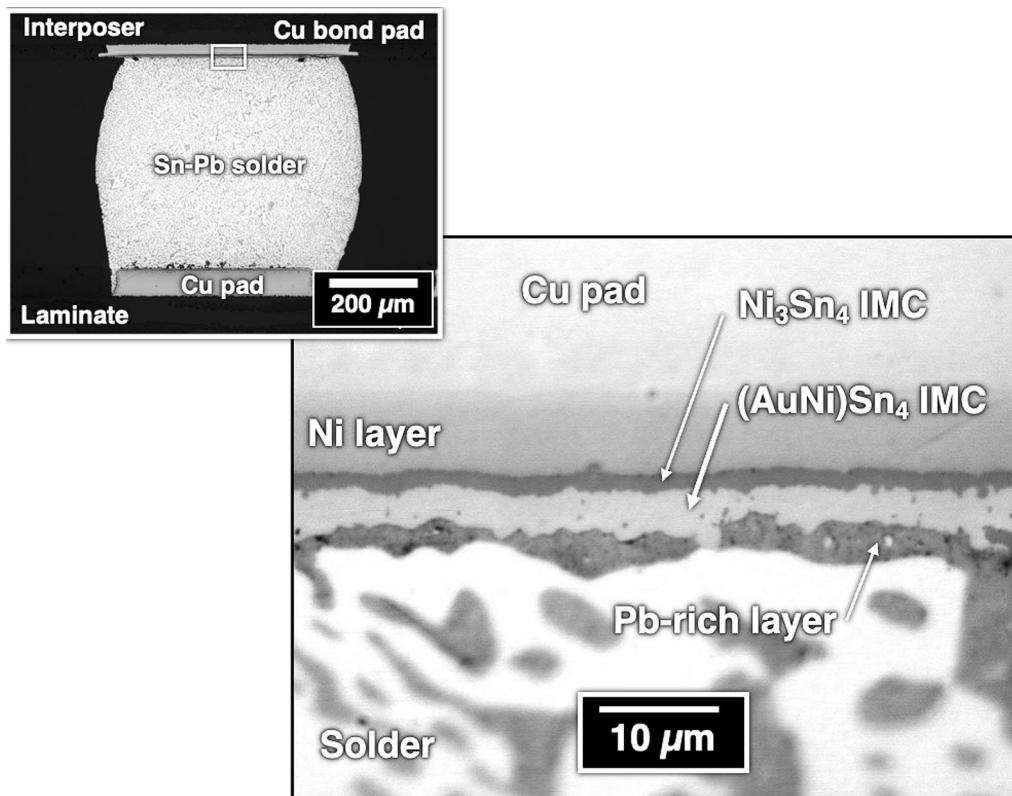


**Fig. 2** Optical micrograph shows the interface microstructure that developed along the Cu bond pad of a BGA solder joint (white box, inset image) resulting from the “return of Au” phenomenon. The sol-

der joint underwent 750 thermal cycles ( $-55^{\circ}\text{C}/125^{\circ}\text{C}$ ; 10-min hold times;  $10^{\circ}\text{C}/\text{min}$  ramp rates).

the thin Au layer of  $0.05\text{--}0.2\ \mu\text{m}$ .<sup>4,6</sup> Consequently, the limited thickness ensured that the Au concentration would not exceed the 4 wt.% limit in most surface-mount solder joints.

However, the ENIG surface finish revealed a Au interface embrittlement failure mode. This phenomenon was observed initially by Mei and coworkers when studying the “drop shock” reliability of ball-grid array (BGA) solder joints and became the subject of several follow-on studies.<sup>7,8</sup> The underlying mechanism was termed “return of Au.” Gold, which had dissolved into the solder during soldering, returned to the Ni solderable layer by solid-state diffusion through the solder joint. The optical micrograph in Fig. 2 illustrates the resulting interface microstructure, which in this case, was observed on the interposer bond pad

belonging to a BGA solder joint after 750 thermal cycles ( $-55^{\circ}\text{C}/125^{\circ}\text{C}$ ; 10 min hold times;  $10^{\circ}\text{C}/\text{min}$  ramp rates).<sup>9</sup> The IMC layer composition was  $(\text{AuNi})\text{Sn}_4$  as measured by electron probe microanalysis (EPMA). The Pb component of the solder, which did not participate in the interface reaction, was rejected from the  $(\text{AuNi})\text{Sn}_4$  IMC layer, forming a Pb-rich layer between the latter and the Sn-Pb solder.

The reference 9 study also identified an ancillary failure mode associated with the return of Au behavior, and specifically, the Pb-rich layer. This failure mode was particular to a thermal cycling environment. The Pb-rich layer became the preferred path for thermal mechanical fatigue (TMF) crack propagation. The consequence was a pronounced reduction in the fatigue lifetime of the solder joint.

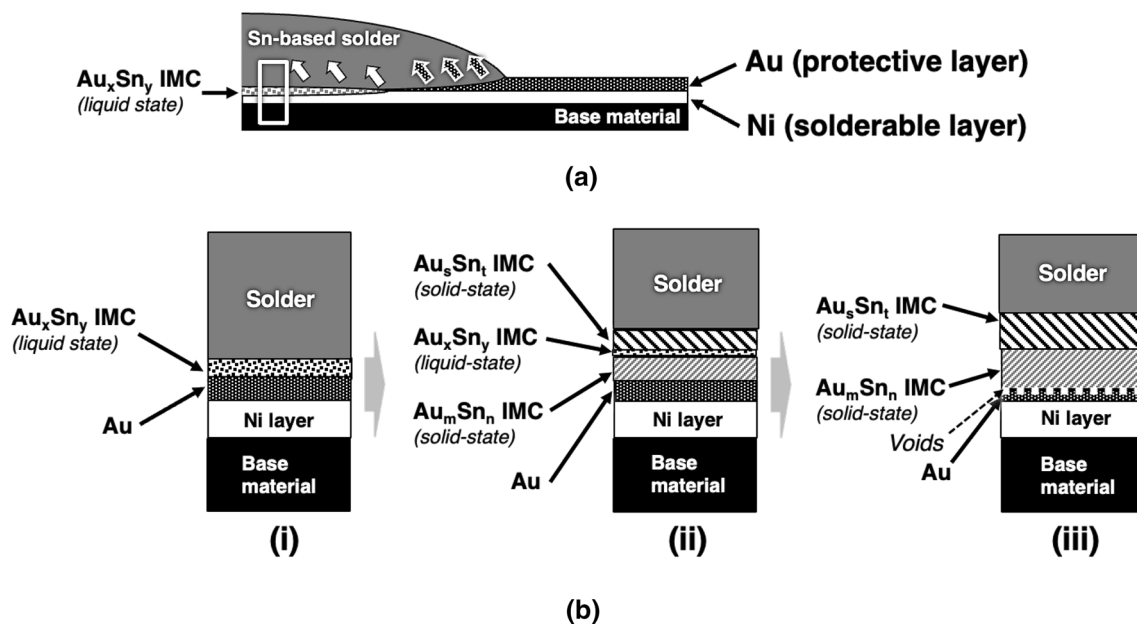


**Fig. 3** Schematic diagrams illustrate the evolution of the interface microstructure resulting from a retained Au layer. (a) The wetting and spreading of solder, which is responsible for the starting microstructure, leaves a Au layer. A section of the interface is identified by the

white box. (b) The sequence of schematic diagrams, i, ii, and iii, illustrate the solid-state evolution of the interface microstructure, which includes Kirkendall void formation (dashed line).

### Soldering Process and Au Interface Embrittlement

The Au protective layer is meant to be completely dissolved into the molten solder (Fig. 1). The opposite scenario was considered, that is, when the Au layer was *not* completely removed by the soldering process. Potential causes include (a) a small solder volume, (b) an overly thick Au layer, (c) a short soldering time (e.g., hand soldering), and/or (d) a low soldering temperature. The starting interface microstructure is illustrated schematically in Fig. 3a. The response of the interface microstructure to solid-state aging is illustrated by the sequence of schematic diagrams, (i)–(iii), in Fig. 3b. The (i) diagram shows a section of the post-solidification microstructure in (a). The  $Au_xSn_y$  IMC layer formed between the Au layer and molten Sn-Pb solder.<sup>1</sup> Solid-state diffusion and reaction processes resulted in the development of two individual  $Au_mSn_n$  and  $Au_5Sn_t$  IMC layers as illustrated in the (ii) diagram. Tin atoms diffuse from the solder through the  $Au_5Sn_t$  IMC and  $Au_xSn_y$  IMC layers to combine with Au atoms and form the  $Au_mSn_n$  IMC layer at the Au/ $Au_xSn_y$  IMC layer interface. At the same time, Au atoms diffuse

from the Au layer through the  $Au_mSn_n$  and remaining  $Au_xSn_y$  IMC layers to combine with Sn to form the  $Au_5Sn_t$  IMC layer at the latter's interface with the solder.

Additional aging, which leads to the schematic diagram (iii) in Fig. 3, accentuates the effects of different diffusion rates between Au and Sn, which is that Au diffuses faster than Sn. The resulting mass transport imbalance creates vacancies to maintain conservation of mass. Those vacancies combine to form Kirkendall voids along the Au/ $Au_mSn_n$  IMC interface. The Kirkendall voids are indicated by the dashed line in (iii). The void concentration increases until it is sufficient to interrupt Au and Sn diffusion, which brings further growth of the  $Au_mSn_n$  IMC layer to a halt and so, too, additional Kirkendall void development. However, typically at this point, the Kirkendall void concentration is sufficient to degrade the mechanical integrity of the solder joint.

Empirical evidence of this interface embrittlement scenario is shown in Fig. 4. A Sn-Pb solder joint was made to a Ni-plated, Cu base material. The electroplated Au protective layer was not fully dissolved by the soldering process. The original  $Au_xSn_y$  IMC layer evolved by solid-state aging into separate layers of the  $Au_5Sn_t$  and  $Au_mSn_n$  IMCs. At the same time, an extensive network of Kirkendall voids formed along the interface between the  $Au_mSn_n$  IMC layer and Au layer. The void concentration was sufficient to result in a mechanical failure of the associated lap joints.

The metastability or pseudo-equilibrium nature of interfaces limits the ability to predict their composition and

<sup>1</sup> A recent study (S. Prasad, P. Kotula, and P. Vianco, "Gold Embrittlement of Pb-Sn Solder Joints: In Situ TEM Heating Studies," manuscript in preparation) using a hot-stage transmission electron microscope (TEM) suggested that that  $Au_xSn_y$  IMC layer was a combination of the AuSn and AuSn<sub>2</sub> phases.

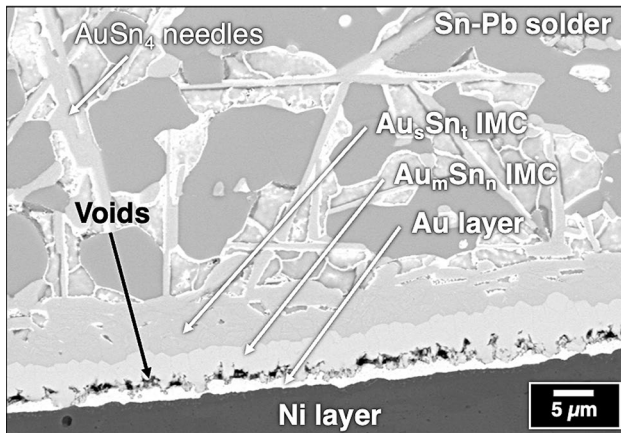


**Fig. 4** SEM photograph shows the formation of Kirkendall voids as a result of solid-state aging and a retained Au layer. The IMC phases correlate with the schematic diagrams in Fig. 3b.

thickness based upon equilibrium constructs such as binary and ternary alloy phase diagrams. Therefore, the present study was undertaken to empirically document the interface microstructure when the Au protective layer is not completely dissolved away. This report, Part 1, examined the evolution of an interface microstructure comprising Au-Sn IMC phases and Kirkendall voids as a function of solid-state aging. The follow-on report, Part 2, will provide a quantitative assessment of the Au-Sn IMC layer composition using the EPMA technique.

This study used the eutectic Sn-Pb solder. Lead (Pb)-bearing solders are no longer suitable for consumer electronics because of environmental regulations. Moreover, the consumer electronics industry has steered primarily towards pure Sn finishes as the Pb-free alternative for component input/output (I/O) structures. Immersion Sn, immersion silver (Ag), or one of the organic solderability preservatives (OSPs) have replaced the Sn-Pb hot-air solder leveled (HASL) surface finish for printed circuit boards in consumer electronics.

On the other hand, the high-reliability electronics industry, which is responsible for military, aerospace, and satellite systems, still relies heavily on eutectic Sn-Pb solder and will do so for the immediate future. Furthermore, this electronics sector makes extensive use of Au protective finishes (electroplated and electroless soft and hard Au layers) on component I/O structures and immersion Au (as part of the ENIG and ENEPIG finishes) on printed circuit boards. The combination of Sn-Pb solder and Au finishes have been documented to result in the aforementioned, interface embrittlement failure modes.

The authors understand that the interface microstructures and rate kinetics of solid-state IMC development are likely to differ between the Sn-Pb solder and the tin-silver-copper

(Sn-Ag-Cu or “SAC”), Sn-Ag-bismuth (Bi), as well as the Sn-Bi low temperatures solders when used in combination with Au finishes. Nevertheless, while relevant, explicitly, to the high-reliability electronics industry, this study can also serve as a baseline resource with which to address potential Au interface embrittlement failure modes associated with Pb-free solders.

## Experimental Procedures

### Test Specimen Materials

The test samples began as Fe-Ni-Co alloy coupons measuring 2.54 cm on a side and 0.254 mm thick. The coupons were electroplated with a Ni solderable layer, nominally 3.5–4.0  $\mu\text{m}$  thick, followed by the Au (protective) layer. The targeted Au thickness was 10  $\mu\text{m}$  thick. The measured Au thickness was  $11.2 \pm 0.3 \mu\text{m}$  (mean,  $\pm$  one standard deviation). This thickness ensured that a sufficient layer remained after soldering to assess the effects of solid-state aging.

The solder was the 63Sn-37Pb (wt.%) eutectic alloy, abbreviated Sn-Pb, and started in the form of solder balls. Three solder ball sizes were evaluated: 25 mg, 100 mg, and 200 mg. The final solder ball size was selected, based on the interface microstructures that are described in the Results section.

### Test Specimen Fabrication

The test specimens were fabricated on a hot plate. The coupon was set on an aluminum sheet. A drop of rosin-based, mildly activated (RMA) flux was placed on the coupon surface followed by the 63Sn-37Pb (wt.%) solder ball. The assembly was transferred to the hot plate. Upon melting, the solder was allowed to wet and spread for 10 s. The soldering temperature was 217°C. Afterward, the aluminum sheet and test specimen were removed from the hot plate and allowed to air-cool. The sample was cleaned of flux residues.

### Aging Parameters

Solid-state aging used temperatures of 55°C, 70°C, 85°C, and 100°C. The aging times are listed below for each temperature:

- 55°C; 5 days and 40 days
- 70°C; 5 days and 40 days
- 85°C; 5 days, 25 days, and 40 days
- 100°C; 5 days, 25 days, and 40 days.

These combinations of times and temperatures represented an acceleration of service environments that are

typical for high-reliability electronics.<sup>2</sup> The aging temperatures remained sufficiently low to avoid the activation of irrelevant diffusion and/or reaction mechanisms.

The test samples were evaluated in the as-fabricated condition, which was by definition, within 1 week following fabrication, to select the solder mass. The baseline condition was established by having all test samples aged at 25°C for 28 days to ensure a consistent starting point in light of the rapid diffusion activity by the Au-Sn system, even at room temperature.

### Microanalysis Methods

Metallographic cross sections were prepared of each sample. The scanning electron microscope (SEM) documented the interface microstructures. The energy dispersive x-ray (EDX) technique provided a qualitative description of the IMC composition. Both instruments were operated at 20 kV. The backscattered electron (BSE) imaging mode was preferred because it accentuated the IMC phases.

The SEM and EDX analyses were performed at three locations: both edges of the sessile drop, which represented the thin solder layer, and at the sessile drop center that represented an “infinitely” thick solder layer. Consistent magnifications were used to document the respective interface microstructures.

## Results

### Solder Ball (Mass) Effect: Bulk Solder and Interface Microstructures

The interface microstructures were examined as a function of the solder quantity (25 mg, 100 mg, and 200 mg Sn-Pb solder balls) to address the possibility that the initial interface was sensitive to the amount of solder. The data informed the selection of a single solder ball size with which to continue the study.

A visual inspection was made of the test pieces. As expected, the wetting and spreading area increased with the amount of solder. Nevertheless, the surfaces exhibited similar morphologies that implied that each one experienced comparable solidification rates.

Figure 5a, b, and c show the center location of the sessile drops formed by the 25 mg, 100 mg, and 200 mg solder balls, respectively. The black arrow and dashed line mark off a distance of 320  $\mu\text{m}$  from the interfaces in order to compare the solder and interface microstructures over a

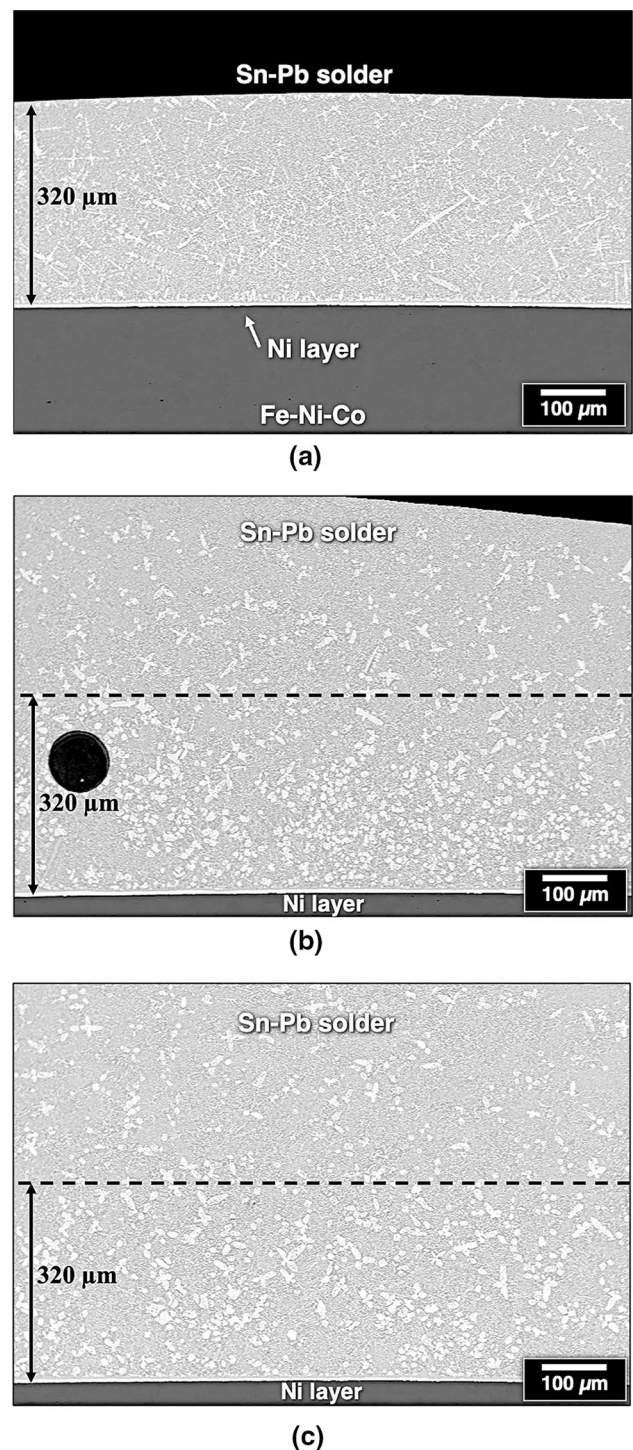


**Fig. 5** SEM photographs show cross sections of the sessile drops as a function of solder quantity at the thick solder layer (sessile drop center): (a) 25 mg, (b) 100 mg, and (c) 200 mg. Arrows and dashed lines mark a common distance of 320  $\mu\text{m}$  from the interface.

similar size scale. Figure 5a (25 mg) shows a portion of the Pb-rich phase as elongated particles distributed uniformly within that 320  $\mu\text{m}$  zone. Only a few of those particles were

<sup>2</sup> Unpublished data, Sandia National Laboratories, Albuquerque, NM. These data and the analysis are available upon request.

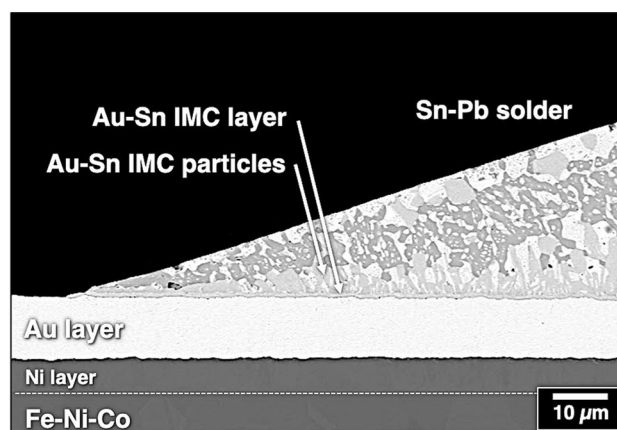
associated with Au-Sn IMC needle-shaped particles. Figure 5b shows the center microstructure of the 100 mg sessile drop. The Pb-rich phase developed only a globular morphology in the 320  $\mu\text{m}$  zone. The Au-Sn IMC particles had both blocky and needle shapes within that zone; their concentrations diminished rapidly beyond the marker. Figure 5c shows the center of the 200 mg sessile drop. The features were similar to those of the 100 mg solder quantity (Fig. 5b).

Using the Pb-rich phase as a microstructural “marker,” the primary difference was observed between the 25 mg sessile drop, which exhibited elongated Pb-rich particles versus the 100 mg and 200 mg test samples that showed Pb-rich particles having a globular morphology. Two possible causes were identified for this difference: (a) the dissolved Au directly altered the driving force controlling Sn-Pb solidification or (b) Au caused a constitutional solidification effect in the 25 mg sessile drop that was absent from the other two test samples. Although the more likely scenario could not be determined from the image data sets, a general conclusion was drawn that the slightly different Pb-rich phase morphologies did not identify a significant microstructural variation that would affect the interface during solid-state aging.

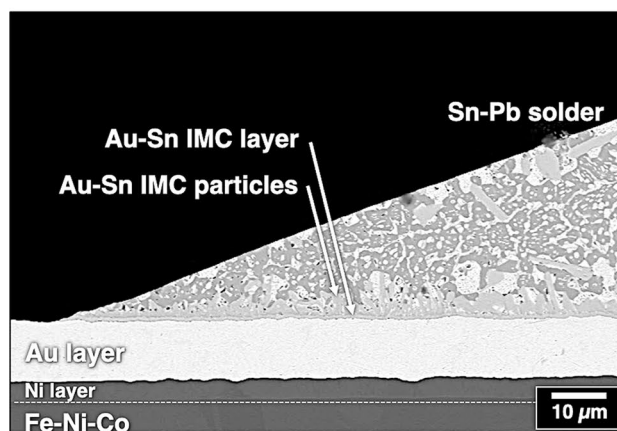
Next, the interface microstructures were examined between the three solder ball sizes. The analysis began with the edge location. The corresponding SEM images are shown in Fig. 6a, b and c. All three samples exhibited a continuous Au-Sn IMC layer adjacent to the remaining Au layer. Columnar particles were observed as a separate IMC phase next to the solder for samples fabricated with the 25 mg and 100 mg solder balls (Fig. 6a and b, respectively). That same IMC phase was present with the 200 mg solder ball, but as particles having both columnar and blocky morphologies (Fig. 6c). The difference was not especially dramatic.

The interface microstructures, which formed at the center locations, are shown in Fig. 7. Again, all three sessile drops exhibited a continuous Au-Sn IMC layer adjacent to the remaining Au layer. The Au-Sn IMC particle phase showed the same sensitivity to solder mass as was observed at the sessile drop edge, that is, columnar particles dominated the 25 mg (Fig. 7a) and 100 mg (Fig. 7b) test samples while both columnar and blocky particles formed in the 200 mg sample (Fig. 7c).

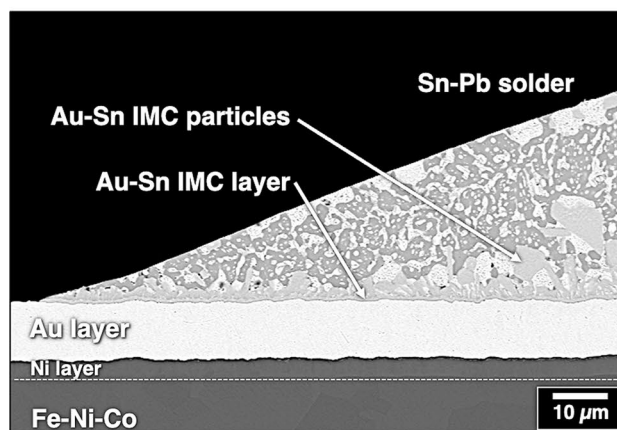
A phenomenon was observed which was associated with the electroplated Ni layer beneath the Au layer. Referring to Fig. 7, the remaining Au thickness was ranked from thickest to thinnest in the order of Fig. 7b (100 mg), Fig. 7a (25 mg), and Fig. 7c (200 mg). A light phase appeared in the Ni layer (white ovals); its prevalence correlated inversely to the remaining Au thickness: absent from Fig. 7b, intermittent in Fig. 7a, and extensive in Fig. 7c. The lighter gray tone suggested the diffusion of Au into the Ni layer. Unfortunately, the EDX analysis did not have the resolution to confirm this scenario. The suspected Au diffusion was absent from



(a)



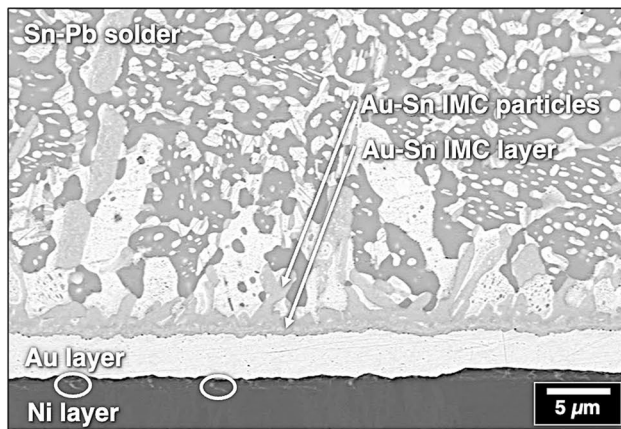
(b)



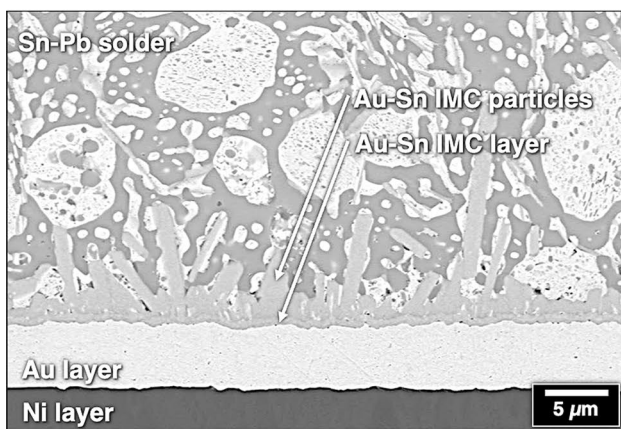
(c)

**Fig. 6** SEM images show the Sn-Pb and interface microstructures under the thin solder layer (sessile drop edge) that were formed by the three solder ball sizes: (a) 25 mg, (b) 100 mg, and (c) 200 mg. The test samples were in the as-fabricated condition.

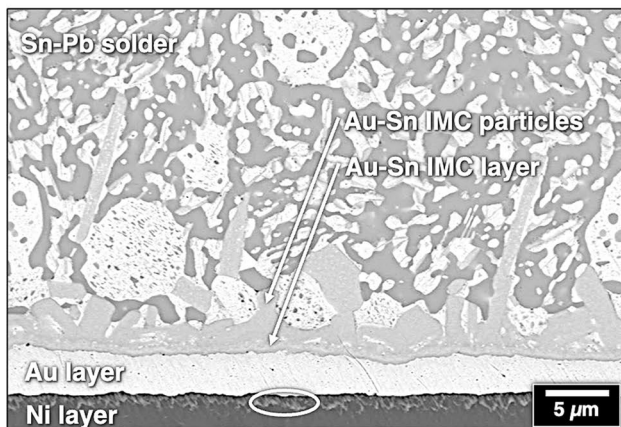
all edge sites, presumably because of the relatively thick Au layer. These trends suggested that the driving force for



(a)



(b)



(c)

**Fig. 7** SEM images show the Sn-Pb and interface microstructures under the thick solder layer (sessile drop center) that were formed by the three solder ball sizes: (a) 25 mg, (b) 100 mg, and (c) 200 mg. The test samples were in the as-fabricated condition. The white ovals identify suspected Au diffusion into the Ni layer.

the suspected Au diffusion into the Ni layer increased with decreasing thickness of the Au layer.

A summary was compiled of the observations derived from Figs. 5, 6, and 7. The images in Fig. 5 show that the near-interface microstructures (320  $\mu\text{m}$  zone) exhibited only a slight variation to the Pb-rich phase morphology versus solder quantity. At both the edge and center locations (Figs. 6 and 7, respectively), a contiguous Au-Sn IMC layer was consistently present above the Au layer for all three solder masses. The Au-Sn IMC particle phase, which was adjacent to the Sn-Pb solder, showed only a columnar morphology with the 25 mg and 100 mg solder ball samples, but had both columnar and blocky morphologies with the 200 mg solder ball specimen. Nevertheless, these two variations would not significantly alter the interface's response to solid-state aging.

Next, the sensitivity of Kirkendall void development was investigated as a function of solder mass and sessile drop location. Figure 8a provides an SEM image of the sessile drop edge resulting from the 100 mg Sn-Pb solder ball. The white box identifies the location of the high-magnification image in Fig. 8b, which showed numerous Kirkendall voids formed along the interface between the contiguous Au-Sn IMC layer and remaining Au layer (black arrows). A similar image pair was taken at the center of the sessile drop; see Figs. 8c and d. Only a few Kirkendall voids formed along the same interface (black arrows). These SEM images indicated that a greater propensity of Kirkendall void formed under the thin solder layer at the sessile drop edge than under the thicker solder layer at the center. The same trend was observed with the 25 mg and 200 mg test samples.

An additional trend was observed whereby the Kirkendall void concentrations were qualitatively similar between the 25 mg and 100 mg solder masses at both locations. However, the 200 mg solder mass produced far fewer voids at the two locations. A review was conducted of the three sessile drop geometries. The edge location was thinner for the 25 mg case. The thickness was not significantly different between the 100 mg and 200 mg masses at their respective edge locations. At the center location, solder thickness increased with solder ball mass, but only slightly so that the difference was negligible vis-a-vis the status of “infinitely” thick layers. Therefore, the small variations of sessile drop profiles did not explain the reduced Kirkendall void presence in the 200 mg test sample. The hypothesis was proposed that this trend was simply a stochastic variation of the interface microstructure generated at the end of the soldering process.

### Solder Quantity (Mass) Effect: Remaining Au Thickness

The extent of Au layer dissolution was determined as a function of solder ball mass by measuring the thickness of

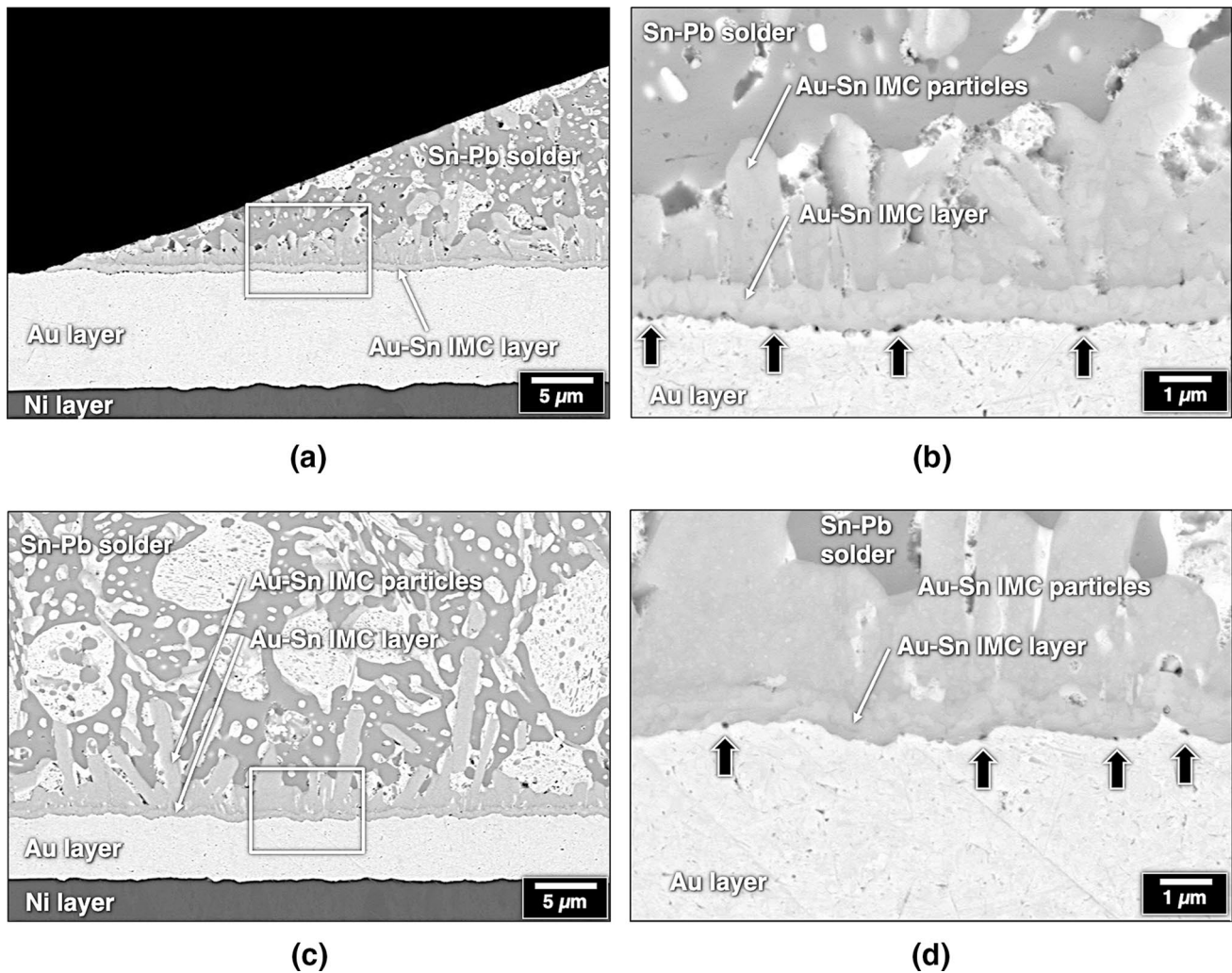


**Fig. 8** Low- and high-magnification SEM images document the as-fabricated interface microstructures created by the 100 mg solder ball: (a), (b) thin solder layer and (c), (d) thick solder layer. The white

boxes in (a) and (c) identify the locations of the high-magnification images in (c) and (d), respectively. The black arrows in the (b) and (d) images identify Kirkendall voids.

the remaining Au layer. The thickness data were obtained at three locations: (a) the unsoldered sites, which established an as-received thickness value; (b) the sessile drop edge; and (c) the sessile drop center. Figure 9 shows the plot of remaining Au layer thickness as a function of the solder mass for both edge and center locations. The as-received Au thickness was  $11.2 \pm 0.3 \mu\text{m}$ , which was represented as a range by the dashed lines demarcating  $\pm 1$  standard deviation about the mean. Gold dissolution was negligible at the sessile drop edges because the limited thickness of solder quickly became saturated with Au. The edge geometry also restricted the exchange of that Au-laden solder with fresh molten solder from the sessile drop center, which further reduced the driving force for dissolution. Lastly, premature constitutional solidification cannot be ruled out as a contributing factor.

More Au layer dissolution occurred at the sessile drop center, which reduced the Au thickness to slightly less than one half of the as-received value. The larger solder thickness maintained the Au concentration below saturation, thereby allowing for additional dissolution and preventing constitutional solidification. The least degree of dissolution (i.e., maximum Au thickness) was observed with the 100 mg solder amount. Thinner Au layers were observed for the 25 mg and 200 mg test specimens, which statistically were similar. A review of the experimental steps did not identify a procedural anomaly responsible for this discrepancy. Moreover, the sessile drop center and its “infinitely” thick solder was expected to have the least variability of Au dissolution between the test specimens. Given the latter premise, a stochastic variability intrinsic to the experimental procedures was likely responsible for



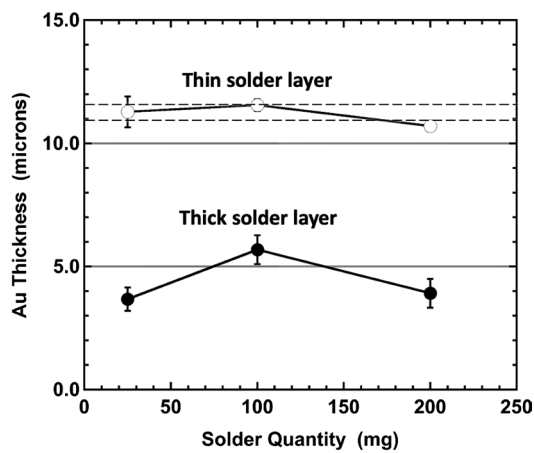


**Fig. 9** Graph shows the thickness of the remaining Au layer as a function of solder ball size used to make the sessile drops. The data are shown for the thin solder layer (sessile drop edge) and the thick solder layer (sessile drop center). The dashed lines indicate the unsoldered Au thickness range established by  $\pm 1$  standard deviation ( $0.3 \mu\text{m}$ ) from the mean ( $11.2 \mu\text{m}$ ).

the observed trend of remaining Au thickness at the sessile drop center.

### Solder Quantity (Mass) Selection

The 100 mg solder mass was selected to construct the test samples for solid-state aging. This solder ball size caused a significant concentration of Kirkendall voids, the occurrence of which was an important objective of this study. Secondly, Fig. 9 indicates that the 100 mg solder quantity maximized the thickness of the remaining Au layer, thereby ensuring that sufficient Au was available for the solid-state interface reactions.

### Baseline Condition: 28 Days at 25°C.

Despite these relatively benign aging conditions, the interface microstructure underwent noticeable changes at both edge and center locations. Figure 10 shows low- and high-magnification SEM image pairs taken at the thick solder layer of the sessile drop center (a, b) and at the thin solder layer of the edge location (c, d). The high-magnification images in Fig. 10b and d were obtained at the white box locations in Fig. 10a and c, respectively. The interfaces at both the edge and center locations exhibited significantly higher Kirkendall void concentrations than were observed for the as-fabricated test specimens (Fig. 8a, b, c and d). Also, the concentration of Kirkendall voids was still higher at the edge location (Fig. 10d) than at the center location (Fig. 10b). In fact, the void concentration at the edge

increased to a degree that it would potentially degrade the interface strength.

A qualitative analysis was made of the thickness of the contiguous Au-Sn IMC layers in Fig. 10b and d. The IMC layer was thicker at the sessile drop edge than at its center. This observation provided a first indication that Kirkendall void concentration was correlated with the growth of this Au-Sn IMC layer.

In summary, the aging parameters of 28 days and 25°C, which established the baseline condition, caused a noticeable increase of Kirkendall voids when compared to the as-fabricated condition. The effect was accentuated at the sessile drop edge where the solder thickness was less and the contiguous Au-Sn IMC layer was slightly thicker versus the center location. These findings indicated a possible correlation between Kirkendall voids, growth of the contiguous Au-Sn IMC layer phase, and the thickness of solder above the interface.

The following hypothesis described the details of this correlation: Kirkendall void formation along the Au/Au-Sn IMC layer interface was a direct result of growth by that Au-rich IMC layer. That IMC layer formed preferentially at the sessile drop edge because the supply of Sn was limited by the thin solder layer. The growth of this Au-rich IMC layer accentuated the mass transport disparity between Au and Sn, thereby generating a higher concentration of Kirkendall voids under the thin solder layer. This scenario directly correlates Kirkendall void formation to solder thickness by means of the Au-rich IMC layer.

The next sections examine the effect of longer term, solid-state aging on the interface microstructure. The discussion was separated into two sections that addressed the thick solder layer (sessile drop center) and thin solder layer (sessile drop edge). Subsections are distinguished by the aging conditions.

### Solid-State Aging: Thick Solder Layer (Center Location)

Figure 11 is a compilation of low-magnification SEM images representing each aging condition, including the baseline sample. The following nomenclature is used to describe the interface microstructural IMC layers in the remainder of this report. The Au-Sn IMC particles eventually coarsened into a continuous layer referred to as the primary (Au-Sn) IMC layer. The contiguous Au-Sn IMC layer, which formed adjacent to the Au layer, is identified as the secondary (Au-Sn) IMC layer. The latter layer was further categorized according to whether it was the “original” layer present in the as-fabricated and baseline samples, or was “new” growth resulting from solid-state aging.

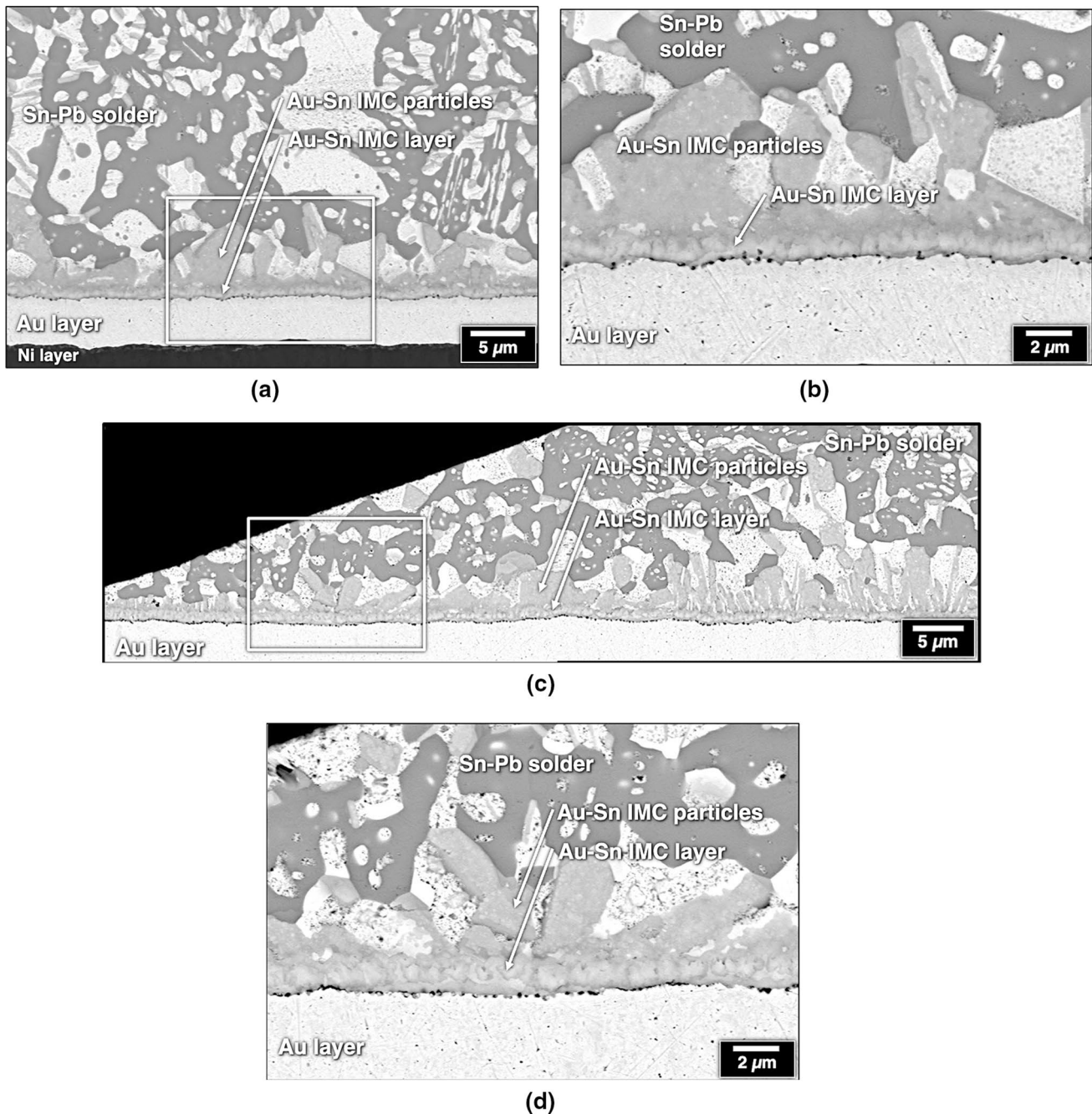


**Fig. 10** Low- and high-magnification SEM images show the interface microstructures representing the baseline condition of post-aging at 25°C for 28 days. The image pairs represent the two solder thick-

nesses: (a), (b), thick solder layer and (c), (d), thin solder layer. The white boxes identify the locations of the high-magnification photographs.

#### **Aged: 55°C, 5 Days and 40 Days**

The original secondary Au-Sn IMC layer experienced slight growth as a function of aging time. The extent of Kirkendall voids remained unchanged after both aging times. A contiguous, primary Au-Sn IMC layer developed with aging time as a result of coarsening by the Au-Sn IMC particles. Concurrent with that coarsening process was the formation

of a Pb-rich layer between the primary Au-Sn IMC layer and Sn-Pb solder as a result of Pb being rejected from the IMC reaction.

#### **Aged: 70°C, 5 Days and 40 Days**

Solid-state aging at 70°C for 5 days resulted in growth of both the primary and secondary Au-Sn IMC layers as

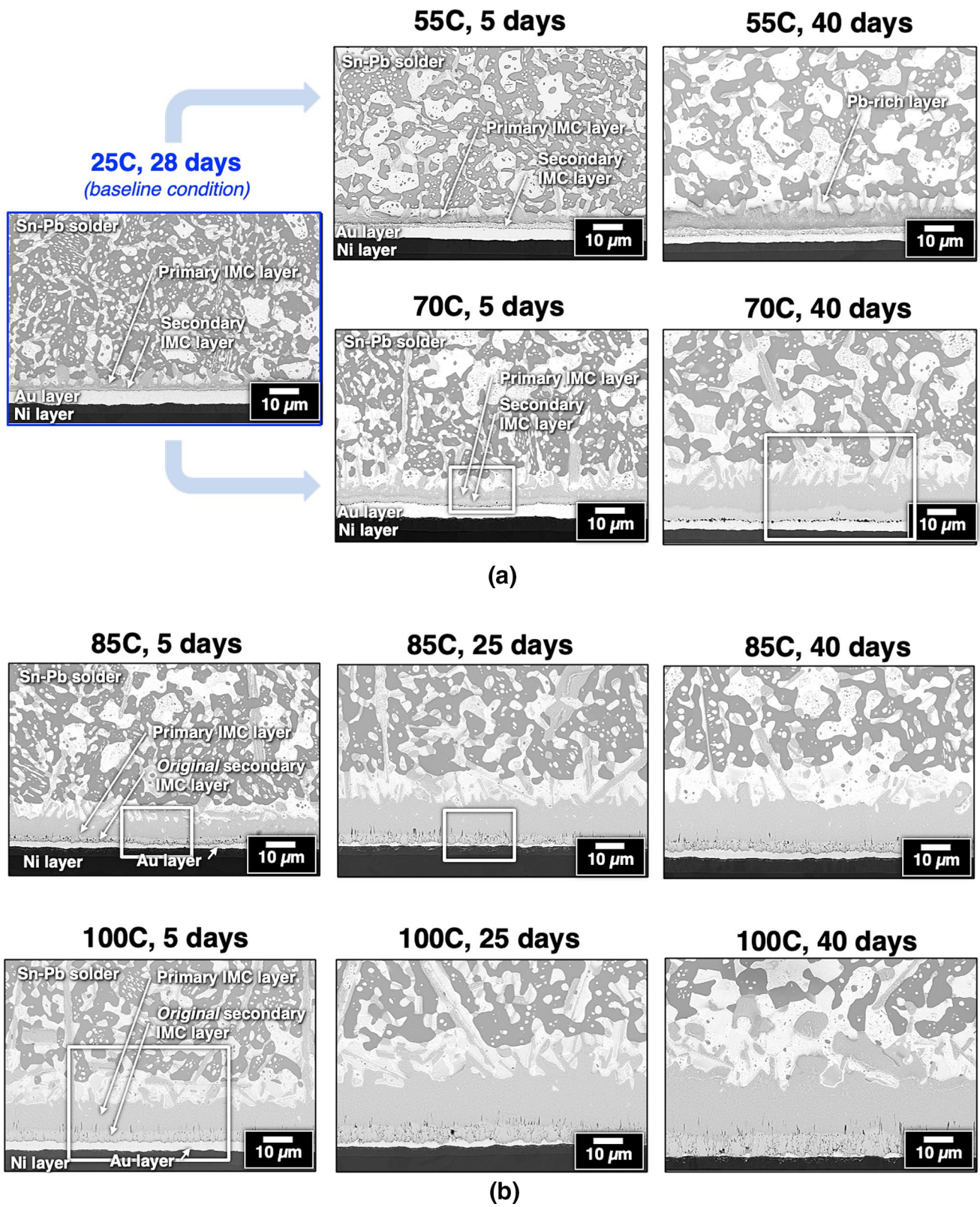
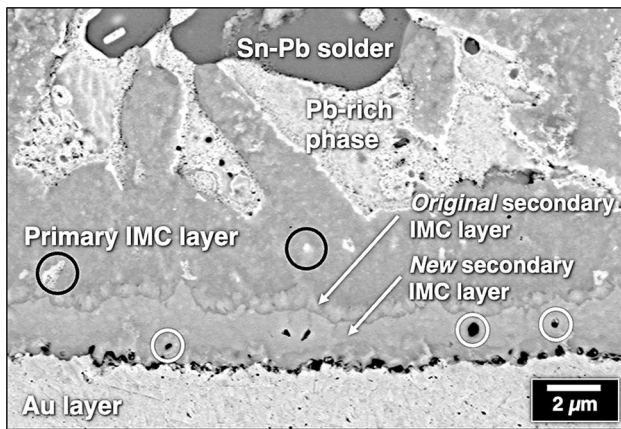
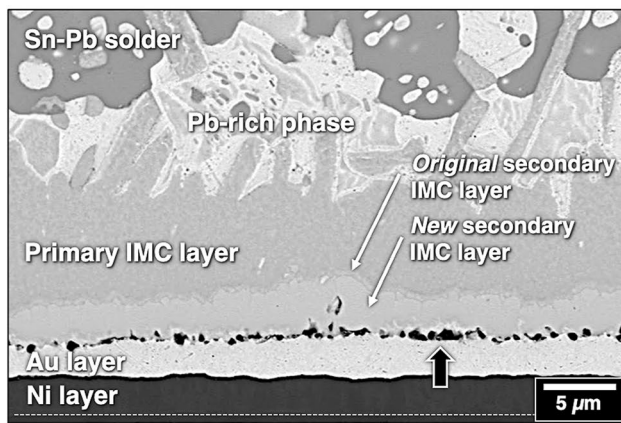


Fig. 11 (a), (b) SEM photographs show the interface microstructures under the thick solder layer representing the baseline and solid-state aging conditions. The white boxes indicate the locations at which higher-magnification images were taken to support the discussion.



(a)



(b)

**Fig. 12** (a) High-magnification SEM photograph shows the interface microstructure under the thick solder layer after aging at 70°C for 5 days. The black circles identify the residual Pb-rich phase. The white circles indicate voids in the secondary Au-Sn IMC layer. (b) High-magnification SEM photograph shows the interface microstructure after aging at 70°C for 40 days (thick solder layer). The black arrow identifies one of several locations where Au was entrapped on the secondary Au-Sn IMC layer side of the Kirkendall voids.

shown in Fig. 11. Higher-magnification photographs were taken at the locations of the white boxes; those images appear in Fig. 12a (70°C, 5 days) and Fig. 12b (70°C, 40 days). Figure 12a shows that the primary Au-Sn IMC layer retained some particle-like morphology; those particles were surrounded by a Pb-rich phase. Several Pb-rich phase particles were entrapped within the primary IMC layer (black circles). The original secondary Au-Sn IMC layer appeared as small grains along the boundary between the new secondary Au-Sn IMC layer and the primary IMC layer. The concentration of Kirkendall voids increased significantly along the Au/secondary Au-Sn IMC layer interface. The extent of voids observed in Fig. 12a would have begun to restrict Sn and Au diffusion across the interface,

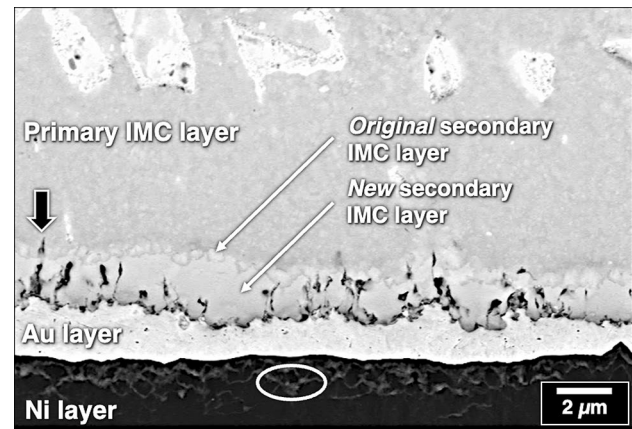


**Fig. 13** SEM image shows the interface microstructure under the thick solder layer after aging for 5 days at 85°C. The black arrow indicates void growth into the primary Au-Sn IMC layer. The white oval identifies Au diffusion into the underlying Ni layer.

leading to a slowing of both secondary IMC layer development and associated Kirkendall voids.

Several Kirkendall voids also formed within the secondary Au-Sn IMC layer (white circles). These voids resulted from the same mechanism based on the dissimilar mass transport rates between Au and Sn. Here, the accumulation points of the vacancies occurred within the IMC microstructure.

Figure 12b provides a high-magnification SEM image of the interface microstructure after aging for 40 days (70°C). Both primary and secondary Au-Sn IMC layers experienced further growth. A significant increase was observed of Kirkendall voids along the Au/secondary Au-Sn IMC interface that jeopardized its integrity.

Gold was observed intermittently on the IMC side of the Kirkendall voids in Fig. 12b—e.g., above the black arrow. The residual Au was not an artifact of the metallographic preparation step. Rather, the accelerated diffusion of Au and Sn caused such a rapid formation of Kirkendall voids that it left the regions of Au entrapped on the IMC side of the interface. An important facet of these observations is that the changes to the interface microstructures depicted in Fig. 12 occurred under the relatively modest aging conditions.

Lastly, Au diffusion into the Ni layer occurred after both aging durations at 70°C. However, its limited extent was barely discernable in the SEM images.

#### Aged: 85°C, 5 Days, 25 Days, and 40 Days

The images in Fig. 11 show an increased thickness of both IMC layers. Kirkendall voids are present along the Au/secondary Au-Sn IMC layer interface, but not to the same extent that followed aging at 70°C and as such would not impede diffusion across the interface. The microstructural features

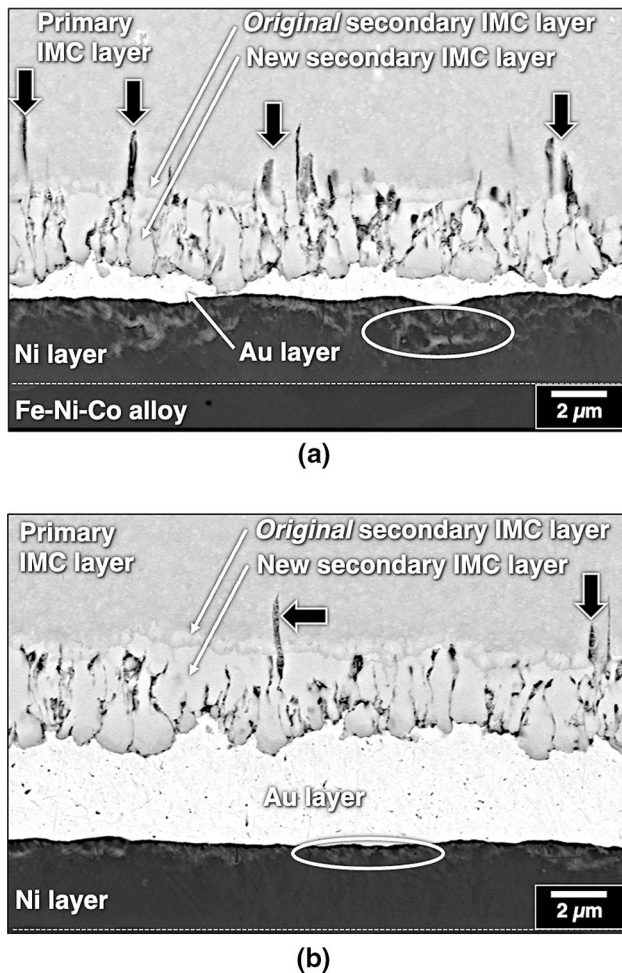


**Fig. 14** SEM images were taken at two locations under the thick solder layer belonging to the test sample aged for 25 days at 85°C: (a) a thin remaining Au layer (yellow box in Fig. 11) and (b) a thick Au layer (not shown in Fig. 11). The black arrows identify void growth into the primary Au-Sn IMC layer. The white ovals identify Au diffusion into the Ni layer.

which formed after aging for 5 days are exemplified by the high-magnification image in Fig. 13 (white box, Fig. 11). The original (secondary) IMC layer remained undisturbed between the primary IMC layer and new growth of the secondary IMC layer. Solid-state aging also generated Kirkendall voids within the secondary Au-Sn IMC layer along its columnar grain boundaries. Grain boundaries provide preferred pathways for Au and Sn diffusion and thus would be particularly susceptible to vacancy accumulation due to the imbalance of their diffusion rates. Some void growth extended into the primary Au-Sn IMC layer (black arrow). The white oval in Fig. 13 identifies Au diffusion into the Ni layer.

The aging time was increased to 25 days. Figure 14a shows the site identified by the white box in Fig. 11. The remaining Au layer was relatively thin. The extension of the

secondary Au-Sn IMC layer became variable into the Au layer. While fewer Kirkendall voids were observed along the Au/secondary Au-Sn IMC interface, their concentration increased significantly within the grain structure of the secondary IMC layer. The “fragmentation” of the layer did not appear to jeopardize its mechanical integrity. Numerous voids also grew into the primary Au-Sn IMC layer (black arrows). Suspected Au diffusion into the Ni layer (white ovals) was confirmed to be such by the EDX analysis.

A second location was identified in the 25-day test sample, which had a relatively thick Au layer. The corresponding SEM image is shown in Fig. 14b. Slightly less Kirkendall void development occurred in both secondary and primary Au-Sn IMC layers (black arrows). A lesser extent of Au diffusion took place into the Ni layer under the thick Au layer (white oval).

The SEM images in Fig. 14 indicate that the interface microstructure and, specifically, Kirkendall void formation within the IMC layers were sensitive to the remaining Au thickness. That sensitivity was not caused explicitly by Au availability since both locations had ample supply of Au to support the interface reactions. The secondary and primary Au-Sn IMC layer thicknesses were not significantly different between the two locations, which suggested that total mass transport of either Au or Sn were not sensitive to the Au thickness. Rather, the Au thickness affected the diffusion rates of one or both elements. The thinner Au caused the Au diffusion rate to increase or the Sn diffusion rate to decrease, thereby enhancing the difference of mass transport rates. The net effect was an increase of Kirkendall void activity observed in Fig. 14a. The conclusion was drawn that the Au thickness altered the driving forces (chemical potential) responsible for Au and Sn diffusion.

Lengthening the aging time to 40 days resulted in thicker Au-Sn IMC layers. Otherwise, similar trends were observed between the remaining Au thickness and Kirkendall void formation within the IMC layers.

#### Aged: 100°C, 5 Days, 25 Days, and 40 Days

The low-magnification SEM images of Fig. 11 show further thickening by the primary and secondary Au-Sn IMC layers. In addition, numerous primary Au-Sn IMC particles formed in the Pb-rich phase.

Figure 15 provides a high-magnification SEM image of the interface microstructure after aging at 100°C for 5 days (white box, Fig. 11). Kirkendall voids formed along the Au/secondary Au-Sn IMC layer interface, but not to an extent that prevented Au and Sn diffusion as confirmed by the thicker IMC layer. Although not readily discernible in the photograph, the original secondary Au-Sn IMC layer was still present between the newly developed layer and the primary Au-Sn IMC layer. Kirkendall voids formed within

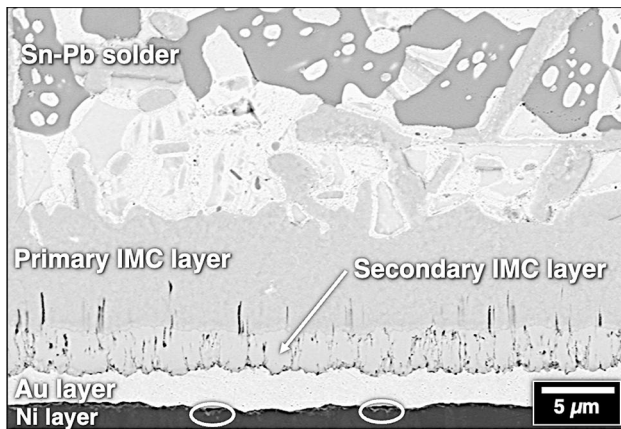


**Fig. 15** SEM image shows the interface microstructure that developed under the thick solder layer after aging at 100°C for 5 days. The white ovals identify Au diffusion into the Ni layer.

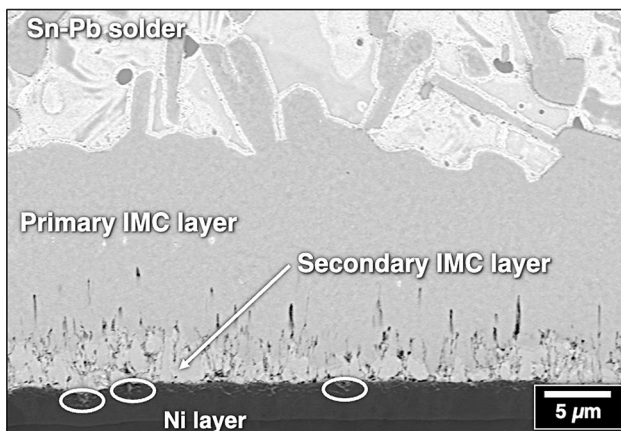


**Fig. 16** SEM image shows the interface microstructure that developed under the thick solder layer after aging at 100°C for 25 days, but where the Au layer was completely consumed by IMC layer development. The white ovals identify Au diffusion into the Ni layer.

the new secondary Au-Sn IMC layer. Numerous voids also developed in the primary Au-Sn IMC layer, but originated along its interface with the original secondary IMC layer. Lastly, a few isolated sites were observed of Au diffusion into the Ni layer (white ovals).

Lengthening the aging time to 25 days caused further thickening of the IMC layers as well as consumption of the Au layer as shown in Fig. 11. In fact, in numerous locations the IMC growth completely consumed the Au layer; see Fig. 16. The secondary Au-Sn IMC layer did not delaminate along its interface with the Ni layer. Both IMC layers experienced internal Kirkendall void development. The original secondary Au-Sn IMC layer was still present.

Several isolated sites in Fig. 16 showed a small degree of Au diffusion into the underlying Ni layer (white ovals). However, where a thicker layer of Au layer remained, this

Au diffusion occurred to a greater extent. At first glance, this trend contradicted the earlier observation that Au diffusion was greater under a thinner Au layer (Fig. 14a vs. 14b). This is because rapid growth of the secondary Au-Sn IMC layer consumed the Au layer before it had the opportunity to diffuse into the Ni layer.

Figure 11 provides an SEM image of the test sample aged for 40 days. The interface microstructure was similar to that following 25 days except for a noticeably thicker secondary Au-Sn IMC layer. The primary IMC layer did not grow significantly thicker. At locations where the Au layer was completely consumed, the interface microstructure was similar to that in Fig. 16 in all aspects, including an absence of delamination along the interface with the Ni layer.

### Solid-State Aging: Thin Solder Layer (Edge Location)

The analysis examined the edge location where a thin solder layer was present above the interface. Negligible dissolution occurred to the Au layer during soldering (Fig. 9). Also, the data showed a posteriori that solid-state aging did not significantly reduce the Au layer thickness. Gold diffusion was not observed into the Ni layer under any aging condition. The discussion below will refer to the SEM images in Fig. 17, which compare interface microstructures across all aging parameters. Additional photographs were provided to illustrate critical points made in the analysis.

#### Aged: 55°C, 5 Days and 40 Days

Referring to Fig. 17, 5 days of aging caused the following changes to the interface microstructure. Coarsening of Au-Sn IMC particles resulted in formation of the primary Au-Sn IMC layer together with the accumulation of Pb-rich phase between the latter and the Sn-Pb solder. The secondary Au-Sn IMC layer experienced a small thickness increase. The extent of Kirkendall voids along the Au/secondary Au-Sn IMC layer interface did not change significantly when compared to the baseline specimen.

The aging time was lengthened to 40 days. The primary Au-Sn IMC layer thickened further as did the accompanying of Pb-rich phase. The details of the secondary Au-Sn IMC layer are shown in Fig. 18a. The uniform thickness of the secondary Au-Sn IMC layer, which was present in the baseline condition, transitioned to an increased degree of variability. The layer grew thicker at some locations (white bracket) while at adjoining sites, only the original secondary IMC layer was observed (black brackets).

Two artifacts of the interface microstructure are documented by the high-magnification SEM image in Fig. 18b that was taken at the white box in Fig. 18a. At the sites where the growth of new secondary IMC layer was absent (black brackets), a high concentration of Kirkendall voids

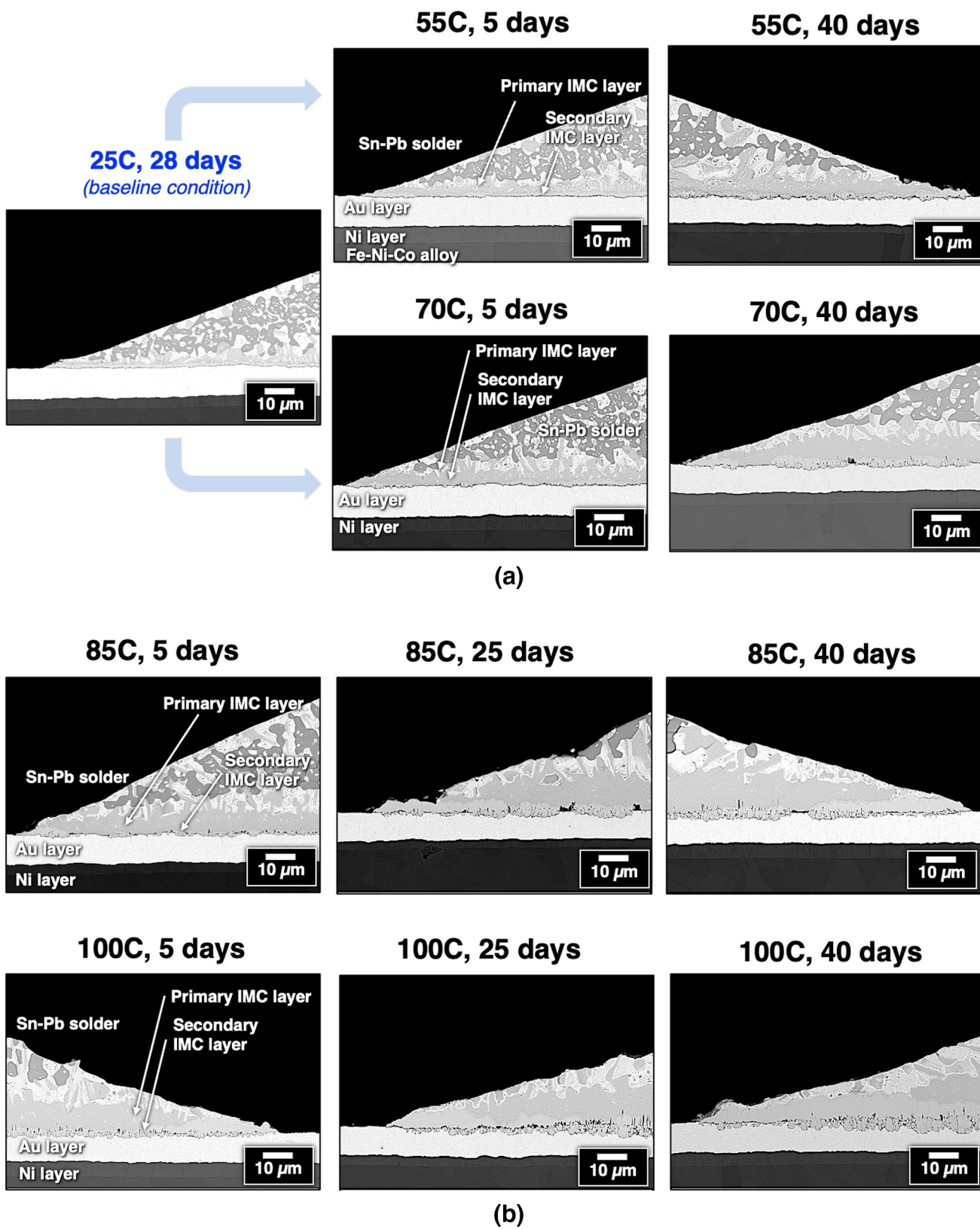
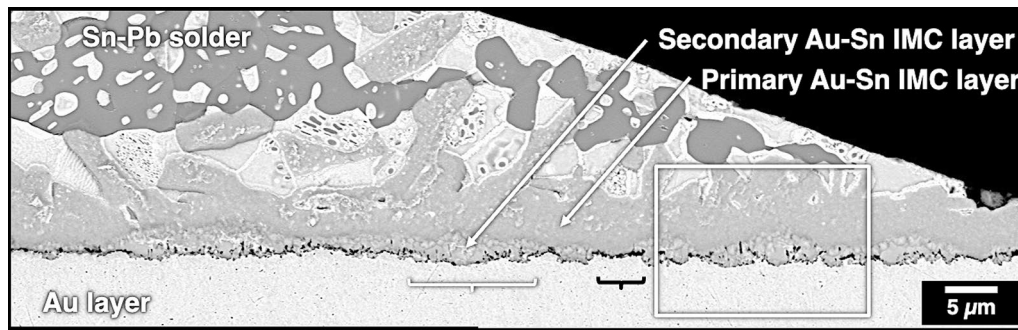
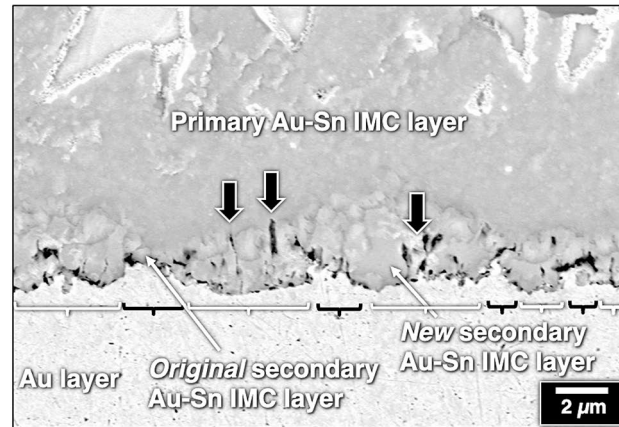


**Fig. 17** (a), (b) SEM photographs show the interface microstructures that formed under the thin solder layer (sessile drop edge) as a function of the solid-state aging conditions and included the baseline condition.



(a)



(b)

**Fig. 18** (a) Montage SEM photograph shows the interface microstructure under the thin solder layer after aging for 40 days at 55°C. New growth of the secondary Au-Sn IMC layer was indicated above the white bracket, but was absent at sites identified by the black bracket. (b) High-magnification SEM image shows in greater detail

the interface microstructure at the white box in (a). The white and black brackets indicate the same features. The black arrows indicate the growth of Kirkendall voids in the secondary IMC layer and beginning to extend into the primary IMC layer.

developed along the interface between the original Au-Sn secondary IMC layer and the Au layer. The thicker Au implied that secondary IMC layer growth ended early in the aging process when the high Kirkendall void concentration interrupted Au and Sn diffusion. At the locations of the white brackets, fewer Kirkendall voids formed at the interface so that Au and Sn diffusion could continue to grow the secondary Au-Sn IMC layer, which extended into the Au layer.

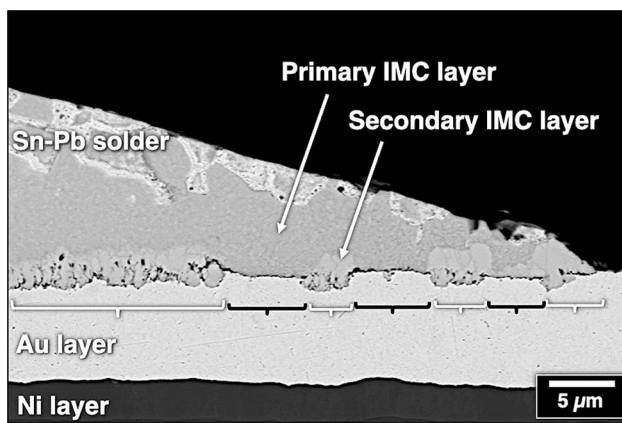
Kirkendall voids also developed within the new secondary Au-Sn IMC layer (black arrows, Fig. 18b). A few voids grew into the primary Au-Sn IMC layer. The long dimension of the voids coincided with the columnar grain structure of the secondary IMC phase. Nevertheless, the increased concentration of Kirkendall voids within the IMC phase did not appear to degrade its structural integrity.

#### Aged: 70°C, 5 Days and 40 Days

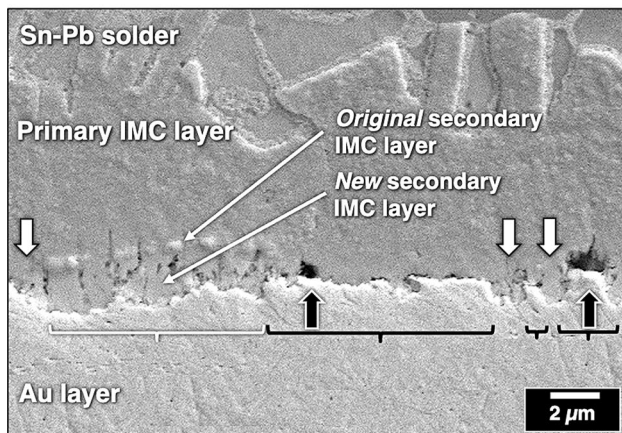
Figure 17 shows the interface microstructure that developed after 5 days. Although the primary and secondary Au-Sn IMC layers were slightly thinner than those that followed 40 days at 55°C, a significantly greater concentration of Kirkendall voids developed along the Au/secondary Au-Sn IMC layer interface.

The aging time was increased to 40 days, resulting in substantial changes to the interface microstructure as shown in Fig. 19a. The primary Au-Sn IMC layer grew thicker. New growth of the secondary Au-Sn IMC layer developed with an intermittent morphology similar to that illustrated in Fig. 18 (55°C, 40 days). The secondary IMC layer grew at the white brackets, which implied that Kirkendall void development at the Au/secondary Au-Sn IMC interface did not impede Au and Sn diffusion.





(a)



(b)

**Fig. 19** (a) SEM photograph shows the thin solder layer under the thin solder layer of the test sample aged at 70°C for 40 days. The secondary Au-Sn IMC layer was present at the white brackets, but absent at the black brackets. (b) High-magnification SEM photograph using the SE image mode to accentuate the original secondary Au-Sn IMC layer. Additional growth of the secondary IMC layer is indicated by the white arrows. The black arrows indicate large Kirkendall voids.

Further analysis was also made of the interface microstructure above the black brackets in Fig. 19a. See Fig. 19b, which was taken using the secondary electron (SE) imaging mode. These regions were characterized by a high concentration of Kirkendall voids that were sufficient to impede Au and Sn diffusion, thereby bringing new growth of the secondary Au-Sn IMC layer to a halt. In addition, several of these locations became accumulation points for vacancies that resulted in large Kirkendall voids (black arrows). This latter artifact was observed in earlier studies of diffusion couples between Au and 50In-50Pb solder.<sup>10–12</sup>

Another observation obtained from Fig. 19b, which was made possible by the SE imaging mode, was that both the original and new secondary Au-Sn IMC phase were absent above the black brackets. This SE imaging mode accentuated the original Au-Sn IMC layer due to the polishing

relief mechanism. The original secondary Au-Sn IMC layer was also absent where new growth was very limited (white arrows). The loss of the original secondary Au-Sn IMC layer and the short-lived growth of new phase occurred because the dominating driving force became that of primary Au-Sn IMC layer growth. The cut-off of the Au supply by Kirkendall voids left the only source of Au as the original secondary Au-Sn IMC layer and any new growth that occurred prior to the interruption of Au diffusion. Therefore, both were consumed by formation of the primary Au-Sn IMC layer.

#### Aged: 85°C, 5 Days, 25 Days, and 40 Days

The interface microstructure, which developed by aging at 85°C, was generally an accentuation of the features observed after aging at 70°C. Figure 20 shows the sessile drop edge after 5 days. The white brackets indicated regions of secondary Au-Sn IMC layer growth. The original secondary IMC layer was also present. Kirkendall voids were observed along the Au/secondary Au-Sn IMC interface, but clearly not to an extent that hindered Au and Sn diffusion. Voids were also observed within the new secondary IMC layer that highlighted the columnar grain structure.

The black brackets in Fig. 20 indicated those interfaces where secondary Au-Sn IMC layer growth had largely ceased and vacancies accumulated into large Kirkendall voids. A few, isolated “bridges” of secondary Au-Sn IMC growth formed into the Au layer (gray areas). Otherwise, the original secondary Au-Sn IMC layer was consumed by additional growth of the primary Au-Sn IMC phase.

The aging time was extended to 25 days, resulting in the interface microstructure shown in Fig. 21. Growth of the secondary Au-Sn IMC layer occurred at the white brackets where Au and Sn diffusion were not cut off by Kirkendall void formation. At the very edge of the sessile drop, the new secondary IMC phase did not contain Kirkendall voids; note the columnar grain structure. The fewer such voids implied a reduction of Au and Sn diffusion and the associated mass transport disparity. Conversely, progressing to the right of the image towards the sessile drop center, new secondary IMC grains developed with an increased presence of voids along the grain boundaries that signified greater diffusion activity. The controlling factor was the solder layer thickness and availability of Sn.

The black brackets in Fig. 21 indicate interface sites where the Kirkendall void concentration stopped both Au and Sn diffusion early in the aging process. The primary IMC layer consumed all of the secondary Au-Sn IMC phase. Several large Kirkendall voids (black arrows) formed as a result of the local accumulations of vacancies.

Forty days of aging (85°C) generated the interface microstructure shown in Fig. 22. Further analysis was performed on the interface microstructure above the solid white

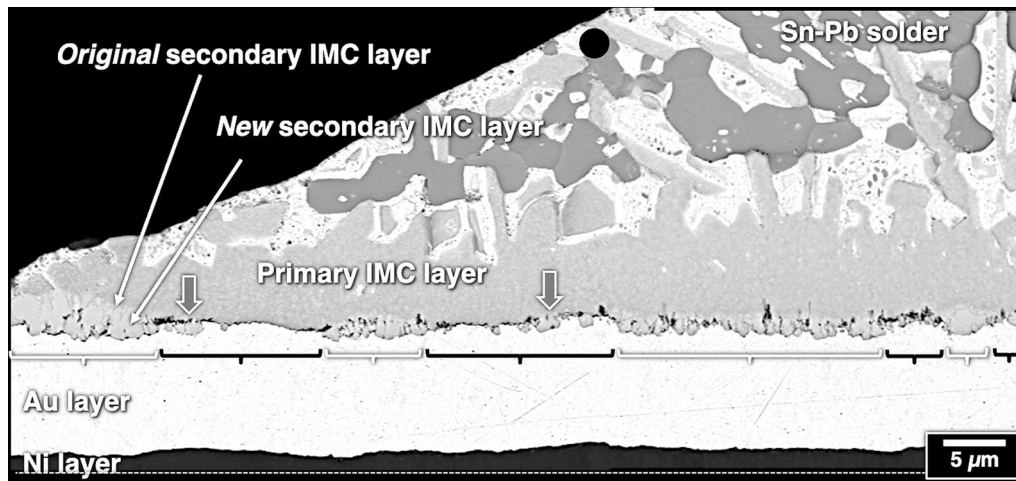


**Fig. 20** SEM montage shows the thin solder layer after aging for 5 days at 85°C. The white brackets indicate regions of secondary Au-Sn IMC growth. Such growth was generally absent from the inter-

face marked by the black brackets except for a few small “bridges” indicated by the gray arrows.

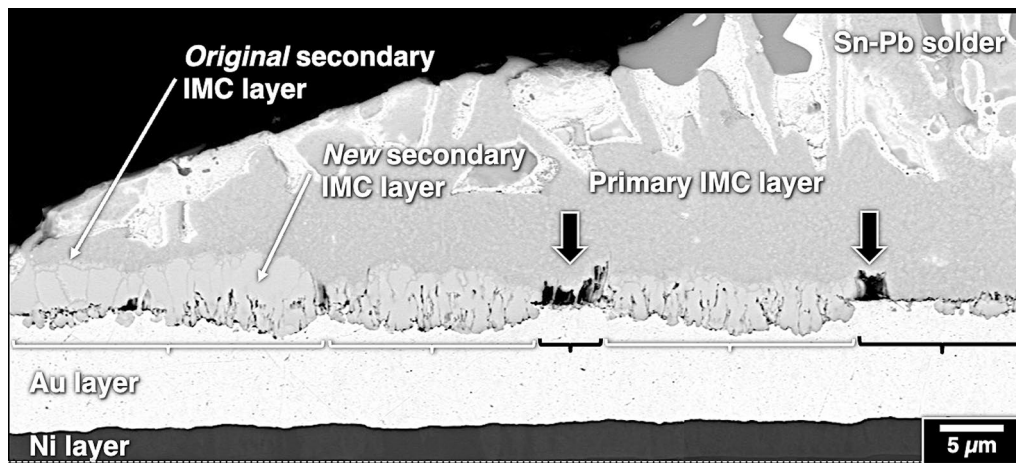


**Fig. 21** SEM montage of the thin solder layer after aging for 25 days at 85°C. The white brackets indicate regions of secondary Au-Sn IMC growth; the black brackets indicate where such growth was generally absent. The black arrows identify sites of large Kirkendall voids.

bracket. First, the limited Sn supply favored growth of the secondary (Au-rich) IMC layer versus the primary (Sn-rich) IMC phase. Note the columnar grain structure. Secondly, three morphologies of growth were labeled at the right side of the image; they are (a) the small grains of the original layer; (b) large grains of new growth without internal Kirkendall voids; and (c) new growth with Kirkendall voids in its columnar microstructure. The new IMC grains, which did not have voids (b), developed later in the aging process when Au and Sn diffusion rates had diminished due to a reduced amount of solder (Sn) remaining above the interface. When the supply of Sn was more ample early in the aging process, Au and Sn diffusion rates, together with the discrepancy between them, were greater, causing an increase

of Kirkendall voids that collected in the new growth of secondary IMC layer (c).

At the site of the dashed black bracket in Fig. 22, a greater thickness of solder—and thus greater supply of Sn—resulted in new growth of the secondary Au-Sn IMC layer. The greater degree of Au and Sn diffusion and, again, the discrepancy between them caused Kirkendall voids to also accompany that growth. However, the total thickness of the secondary IMC layer was less than that above the white bracket because greater supply of Sn also increased growth of the primary Au-Sn IMC layer, which included voids within its microstructure (black arrows).

The black bracket in Fig. 22 identifies the location where Kirkendall voids were sufficient to stop both Au and Sn

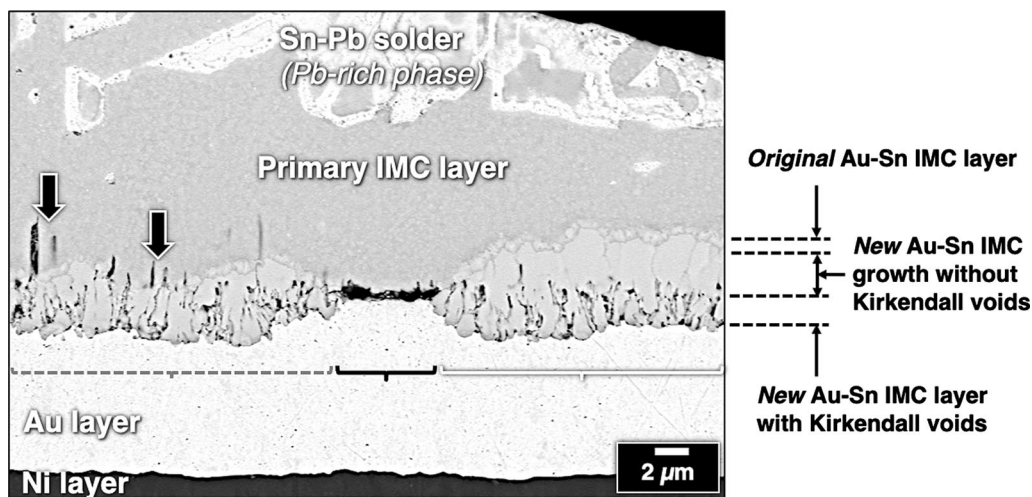


**Fig. 22** SEM image taken at the thin solder layer of the test sample aged for 40 days at 85°C. The white brackets indicate regions of secondary Au-Sn IMC layer growth, the three morphologies of which are identified at the right. The dashed black bracket identifies the Au/secondary Au-Sn IMC layer interface having two of the three mor-

phologies—the missing morphology being new growth without Kirkendall voids. Kirkendall voids developed in the primary Au-Sn IMC layer (black arrows). Evidence of the secondary IMC layer was absent at the black bracket; only a large Kirkendall void was present.

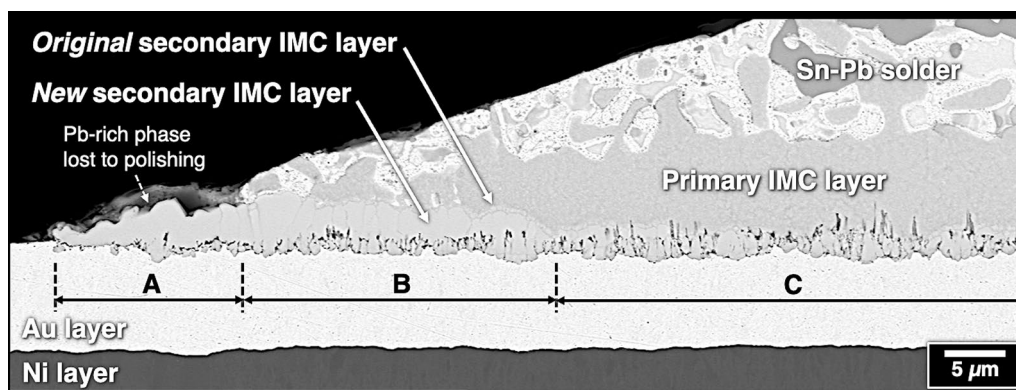


**Fig. 23** Montage SEM image shows the interface microstructure under the thin solder layer after aging for 5 days at 100°C. Three distinct morphologies are identified by the labels “A,” “B,” and “C”.

diffusion across the Au/secondary Au-Sn IMC layer early in the solid-state aging treatment. The consequences were (a) an early end to further development of the secondary Au-Sn IMC layer, which left the thicker Au layer, and (b) the conversion of the original secondary IMC layer to the primary Au-Sn IMC phase.

#### Aged: 100°C, 5 Days, 25 Days, and 40 Days

The interface microstructure experienced a dramatic transition with increased thickness of the solder layer from the sessile drop edge towards its center. This observation is documented by Fig. 23; the aging time was 5 days. Region “A” showed only the secondary Au-Sn IMC phase. The Sn-Pb solder was replaced by Pb-rich phase (that was lost

to the polishing process). The high-Au, secondary Au-Sn IMC composition was preferred due to the lack of Sn and an ample supply of Au. Kirkendall voids formed along the Au/secondary Au-Sn IMC interface and minimally so in the IMC grain boundaries.

Region “B” was characterized by further growth of new secondary Au-Sn IMC layer resulting from a greater supply of Sn. The IMC layer had two morphologies, with and without internal Kirkendall voids. A limited concentration of Kirkendall voids was observed along the Au/secondary Au-Sn IMC interface. The original secondary Au-Sn IMC layer was present at the interface between the two IMC layers.

Region “C” exhibited two distinguishing features. First, the new secondary Au-Sn IMC layer was thinner than at “B.”

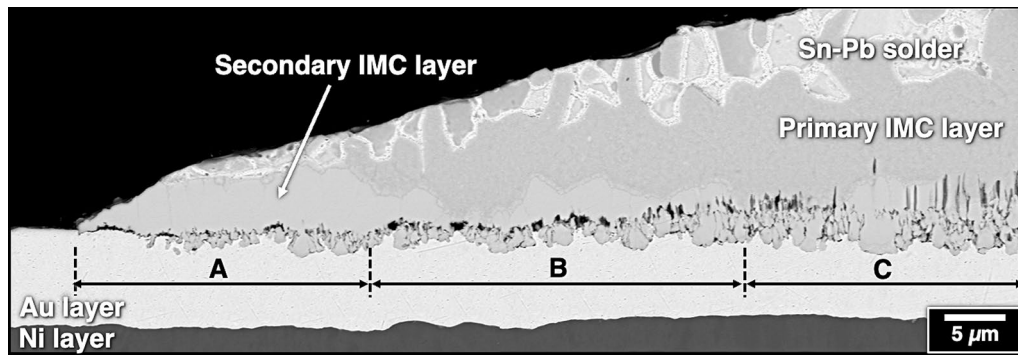


**Fig. 24** Montage SEM image shows the interface microstructure under the thin solder layer after aging for 25 days at 100°C. The three morphologies are labeled “A,” “B,” and “C”.

The thicker solder layer (Sn) caused a decreased preference for secondary IMC layer growth in favor of growth by the primary Au-Sn IMC layer. The secondary Au-Sn IMC morphology contained Kirkendall voids. The second phenomenon was that Kirkendall voids formed in the thickening, primary Au-Sn IMC layer. The original secondary Au-Sn IMC layer was still present along the mutual interface between the two IMC layers. In summary, the interface microstructure trend from Region “A” to “C” indicated an increase of Au and Sn diffusion activity with increased thickness (Sn supply) of the solder. Also, the increased solder layer thickness caused a shift away from the secondary Au-Sn IMC layer to the primary IMC layer.

The discussion will jump to the results of aging for the longest duration, 40 days. The interface microstructure was generally similar to that in Fig. 23 (5 days) except that additional growth by the new secondary Au-Sn IMC phase caused the three regions to extend further towards the thicker solder layer.

The test sample aged for 25 days is shown in Fig. 24. All three regions “A,” “B,” and “C” were present along the interface; however, the boundaries between them were not as distinct as in Fig. 23. Also, region “B” differed from that of the other two aging times by a very limited growth of new secondary Au-Sn IMC phase because of an extensive network of Kirkendall voids. The original secondary Au-Sn IMC layer was still observed between the new growth and the primary Au-Sn IMC layer. Extensive Kirkendall void development occurred within both IMC layers belonging to region “C.” The variable concentrations of Kirkendall voids were responsible for the irregular profile of the Au/secondary IMC interface.

Potential sources were considered for the different trends experienced between 5 days (and 40 days) aging (Fig. 23) versus 25 days (Fig. 24). First, the scenario was considered in which the differences resulted from an explicit time dependence by one or more of the driving forces responsible for the interface reactions and/or Au and Sn diffusion processes.

The basis for such a stipulation lies in the metastable nature of interfaces. A second scenario was that the trends simply reflected the stochastic nature of interface microstructures and the responses to those slight variations to subsequent, solid-state reaction and diffusion processes. Those minor microstructural difference became further accentuated by aging. Regardless of the controlling scenario, these findings documented the variability of the interface microstructures, including Kirkendall void formation, which can characterize the interface adjoining the retained Au layer.

## Discussion

The above data illustrate the changes to the interface microstructure when the Au protective finish was not completely removed by the soldering process. More importantly, those changes occurred under relatively modest temperature and time conditions. Therefore, the interface embrittlement mechanism can be activated relatively *early* in the solder joint life cycle. The potential loss of electrical or mechanical function may take place as an infant mortality failure prior to the system entering service. However, Au interface embrittlement has also been documented to cause latent failures when the assembly is in service. Whether this phenomenon causes an infant or latent failure depends upon, not only the time–temperature history, but also the residual stresses and service loads placed on the solder joint.

This study demonstrated the sensitivity of the interface microstructure and in particular, Kirkendall void formation, to the thickness of the solder layer. Those experiments, which varied the solder quantity (25 mg, 100 mg, and 200 mg), caused only minor variations to the Au-Sn IMC particle phase that would become the primary IMC layer. Similarly, the Au-Sn IMC layer, which would become the secondary Au-Sn IMC layer, was not strongly sensitive to solder mass.

Referring specifically to Kirkendall void development, all three solder quantities showed the same trend: Kirkendall void formation along the Au/secondary Au-Sn IMC layer interface was greater under the thinner solder layer at the sessile drop edge. The differences in the sessile drop thickness profiles were considered to be too small to be responsible for the small Kirkendall void sensitivity to solder ball mass. Rather, the sensitivity to solder mass was simply a stochastic variation between the starting sample conditions.

The dependence of Kirkendall void development on solder thickness was considered with respect to engineering applications. First of all, the Au-Sn IMC phases and their respective morphologies were similar to those documented in actual electronic solder joints that experienced interface embrittlement. See Fig. 4 as an example. Secondly, the sessile drop, solder thickness profile was compared to the gap thickness of typical electronic solder joints. The edge location included a solder thickness range of 25–50  $\mu\text{m}$  (0.001–0.002 in), which is comparable to typical Sn-Pb solder joint clearances. “Infinitely” thick solder would pertain to solder thicknesses in excess of 100  $\mu\text{m}$  (0.004 in.), which were represented by the sessile drop center. A transition region included solder thicknesses in the range of 50–100  $\mu\text{m}$  (0.002–0.004 in.).

Next, the impact was considered by the changing interface microstructures as a function of solid-state aging, beginning with the center location (thick solder layer). A new secondary Au-Sn IMC phase formed with a relatively consistent layer thickness. Kirkendall voids were present at its interface with the Au layer, but not to an extent that jeopardized the integrity of the interface. Kirkendall voids also formed within the new secondary Au-Sn IMC layer and to a lesser extent, grew into the primary Au-Sn IMC layer. The secondary Au-Sn IMC phase’s grain structure was not significantly degraded, despite its fragmented appearance in the SEM images. Lastly, when growth of the secondary Au-Sn IMC layer fully had consumed the remaining Au layer, the resulting secondary Au-Sn IMC layer/Ni interface did not exhibit delamination (e.g., Fig. 16).

As a summary of these observations, the risk of interface embrittlement is low in the presence of a remaining Au layer when the solder thickness exceeds 100  $\mu\text{m}$  (0.004 in.). The low risk stems from these three factors: (a) limited and more uniform secondary Au-Sn IMC layer growth that lessened both the magnitude and variability of Kirkendall void formation at the Au/secondary Au-Sn IMC layer; (b) satisfactory mechanical integrity of the secondary Au-Sn IMC layer despite extensive Kirkendall void formation within it; and (c) adequate adhesion along the secondary Au-Sn IMC layer/Ni layer interface in the event that solid-state IMC growth completely consumes the Au layer.

This applications analysis continued by addressing the thin solder layer. The limited availability of Sn caused the

interface reaction to shift preference for the Au-rich, secondary Au-Sn IMC layer with its accompanying Kirkendall void formation. The higher aging temperatures accelerated Au and Sn diffusion, thereby increasing Kirkendall void formation but unevenly along the interface. At those locations where void formation was particularly severe (black brackets, Figs. 18–22), Au and Sn diffusion were interrupted early in the aging process, which halted secondary Au-Sn IMC layer growth. Two phenomena were observed: First, some locations became accumulation points of vacancies, forming locally large Kirkendall voids. Functionally, the large Kirkendall voids could potentially degrade the electrical and mechanical function of the solder joint if present in sufficient numbers. Second, the loss of access to Au shifted the reaction driving forces to prefer the primary Au-Sn IMC phase, resulting in the conversion of both the original secondary Au-Sn IMC layer and any newly formed IMC layer into the primary Au-Sn IMC phase. This conversion of IMC phases did not appear to degrade interface integrity.

The complementary interface segments (white brackets, Figs. 18–22) had fewer Kirkendall voids along the Au/secondary Au-Sn IMC interface. The reduced void formation allowed additional growth of new secondary Au-Sn IMC phase, which was accompanied by Kirkendall void formation within its columnar grain boundaries. This interface microstructure did not pose the risk of a catastrophic failure.

A summary is compiled of these observations with respect to the thin solder layer. The interface embrittlement mechanism, which is attributed to a retained Au layer, poses a high risk to solder joint integrity with the thin solder layer, that is, a thickness less than 50  $\mu\text{m}$ . The primary mechanism is the accelerated development of the secondary Au-Sn IMC phase, which in-turn, is accompanied by an increased concentration of Kirkendall voids. The solder joint failure mode was exemplified in Fig. 4. An additional risk factor is the variability of the secondary IMC layer growth and thus, the propensity for Kirkendall void formation. This point was also illustrated in Figs. 18–20. When this variability is scaled to increasingly smaller solder joints used in the electronics industry, it causes an increased uncertainty to interconnection reliability.

Recall that numerous center locations experienced Au diffusion into the Ni layer (e.g., Fig. 14). The degree of that diffusion increased with decreasing thickness of the remaining Au layer, hence its greater propensity under the thick solder layer. Mechanisms were discussed whereby the driving force behind the Au diffusion was sensitive to either the Au layer thickness, explicitly, or the increased proximity of the Au/secondary Au-Sn IMC layer interface to the Au/Ni interface as a consequence of the thinner Au layer. While a more in-depth analysis would be interesting to discern the controlling mechanism, such a study was beyond the scope of the present investigation.

Lastly, the retained Au protective layer was correlated with the interface embrittlement failure mode vis-à-vis the solid-state aging conditions. The time and temperature parameters used in the present study were an acceleration of service environments experienced by high-reliability electronic systems. In addition, the elevated temperature conditions that these electronics experience during next-assembly processes as well as qualification and acceptance testing could potentially accelerate these mechanisms, depending on the time–temperature profiles. The Au-Sn IMC layers, themselves, although brittle and in many cases fragmented by in situ Kirkendall void formation, did not appear to pose a high probability for a catastrophic failure. Rather, the principle failure mode was determined by the extent of Kirkendall void formation along the Au/secondary Au-Sn IMC interface.

## Summary

1. A study was performed which examined the interface embrittlement mechanism resulting from a Au protective layer that is not fully consumed during the 63Sn-37Pb (Sn-Pb) soldering process. The sessile drop configuration allowed for examining the role of solder thickness on the interface microstructure as a function of solid-state aging (55–100°C; 5–40 days).
2. The as-fabricated condition had interface Au-Sn IMC structures that included a contiguous layer adjacent to the Au layer, a zone of particles between the contiguous layer and the Sn-Pb solder, and Kirkendall voids along the Au/contiguous IMC layer interface.
3. The aging duration of 28 days at 25°C, which established the baseline condition, caused a noticeable increase of Kirkendall voids along the Au/Au-Sn IMC layer interface versus the as-fabricated condition.
4. Kirkendall void development was coupled to growth of the high-Au, secondary Au-Sn IMC layer.
5. The baseline test samples and those subjected to solid-state aging established the following observation: Kirkendall void development increased along the Au/secondary Au-Sn IMC interface with decreasing solder thickness.
6. When the solder thickness was less than 50 µm, rapid growth of the secondary Au-Sn IMC layer led to an increased extent of Kirkendall voids as well as a greater variability of both structures along the Au/secondary Au/Sn IMC interface. A high risk was present of a catastrophic failure.
7. When the solder thickness was greater than 100 µm, Au and Sn diffusion remained active. Kirkendall voids developed to a more modest degree along the Au/secondary Au-Sn IMC interface; they also formed

within the secondary Au-Sn IMC phase and to a lesser degree, in the primary Au-Sn IMC layer. However, the resulting interface microstructure posed a low risk of catastrophic failure by interface embrittlement.

8. Gold diffusion was observed into the Ni layer, the extent of which increased with decreasing Au thickness. This phenomenon did not pose a risk to solder joint integrity.
9. This study demonstrated that interface embrittlement caused by the incomplete removal of a Au protective finish can potentially lead to infant mortality failures or latent failures after the solder joint has entered service.

**Acknowledgments** The authors wish to thank Dr. Rebecca Wheeling for a thorough review of the manuscript. Sandia National Laboratories is a multi-mission laboratory managed and operated by National Technology and Engineering Solutions of Sandia LLC, a wholly owned subsidiary of Honeywell International Inc. for the U.S. Department of Energy's National Nuclear Security Administration under contract DE-NA0003525. This paper describes objective technical results and analysis. Any subjective views or opinions that might be expressed in the paper do not necessarily represent the views of the U.S. Department of Energy or the United States Government.

**Conflict of interest** The authors declare that they have no conflict of interest.

## References

1. P.T. Vianco, *Soldering Handbook*, 3rd ed., (Miami, FL: American Welding Society, 2000), p. 24.
2. P. Vianco, Understanding the Reliability of Solder Joints Used in Advanced Structural AND Electronics Applications: Part 1, Filler Metal Properties and the Soldering Process. *Welding J. Res. Supp.* 96, 39s (2017).
3. P. Vianco, A Review of Interface Microstructures in Electronic Packaging Applications: Soldering Technology. *J. Metals* 71, 158 (2019).
4. P. Vianco, An Overview of Surface Finishes and Their Role in Printed Circuit Board Solderability and Solder Joint Performance. *Circuit World* 25, 6 (1998).
5. M. Bester, *Proc. Inter NEPCON* (1968), p. 211.
6. IPC-4552B, Specification for Electroless Ni/Immersion Au(ENIG) Plating for Printed Boards, (IPC, Bannockburn, IL, 2021)
7. Z. Mei, P. Callery, D. Fisher, F. Hua and J. Glazer, *Proc. Pacific Rim/ASME International Intersociety Elect. and Photonic Pack. Conf.* (1997) p.1543.
8. J. Davis, M. Bozack, and J. Evans, Effect of (Au, Ni)Sn<sub>4</sub> Evolution on Sn-37Pb/ENIG Solder Joint Reliability Under Isothermal and Temperature-Cycled Conditions. *IEEE Trans. CPT* 30, 32 (2007).
9. Paul T. Vianco, Jerome A. Rejent, J. Mark Grazier, Steven E. Garrett, Sara S. Sokolowski, Gregory L. Dinger, Michael K. Nielsen, Laura L. Halbleib, Alice C. Kilgo and Richard P. Grant, Qualification Program for the Solder Interconnections of Three Area-Array Packages on Copper and Non-Copper

- Core, Multi-Layered Printed Circuit Boards. Sandia Report SAND2015-7495 (Sandia National Laboratories, Albuquerque, NM; 2015).
10. G. Powell and J. Braun, Diffusion in Gold-Indium System. *Trans. AIME* 230, 694 (1964).
  11. F. Yost, F. Ganyard and M. Karnowski, Layer Growth in Au-Pb/In Solder Joints. *Metall. Trans. A* 7A, 1141 (1976).
  12. P. Vianco, G. Bryant, P. Hlava and G. Zender, Interface Reactions Between 50In-50Pb Solder and Electroplated Au layers. *Mater. Sci. and Eng. A* 409, 179 (2005).

**Publisher's Note** Springer Nature remains neutral with regard to jurisdictional claims in published maps and institutional affiliations.